Flame stabilization of oxy-fuel flames

Zegers, R.P.C.

Award date:
2007

Flame stabilization of oxy-fuel flames

R.P.C. Zegers

MSc. Thesis
Report number WVT 2007.13

Supervisors:
dr.ir. M.J. Remie
prof. dr. L.P.H. de Goey

Eindhoven University of Technology
Department of Mechanical Engineering
Division Thermo Fluids Engineering
Section Combustion Technology

Samenvatting

Voor het verhitten van glas worden vaak vlammen gebruikt die pure zuurstof verbruiken in plaats van lucht, omdat dan door de hogere temperatuur en snelheid een hogere warmteoverdracht naar het glas mogelijk is. Hierdoor worden de proces tijden verkort. De warmteoverdracht naar het glas is afhankelijk van de dikte van de viskeuze grenslaag bij het glas. Een dunnere grenslaag zorgt voor een hogere warmteoverdracht. Om de viskeuze grenslaag zo dun mogelijk te krijgen moet de *strain rate* zo groot mogelijk zijn. De *strain rate* is lineair afhankelijk van de snelheid van de verbrande gassen. Dit betekent dat om een zo groot mogelijke warmteoverdracht naar het glas te realiseren, de snelheid van de verbrande gassen zo groot mogelijk moet zijn. Dit kan worden bereikt door een zo groot mogelijke snelheid van de onverbrande gassen. De snelheid van de onverbrande gassen kan echter niet oneindig verhoogd worden, omdat de vlam dan van de brander afblaast. Deze afblaasgradiënt is volgens literatuur niet afhankelijk van de branderdiameter, er is echter geen rekening gehouden met de vorm van de brander in de afblaasgradiënt theorie van Lewis en von Elbe [1].

In de industrie verandert de geometrie van de brander in tijd door vervuiling en slijtage. Deze veranderende geometrie beïnvloedt de stroming en dus het moment van afblazen van de vlam. Dit relateert de afblaaslimiet aan de brander geometrie.

In dit onderzoek is een nieuw inzicht vergaard betreffende de afblaas criteria van methaan-zuurstof vlammen. Verschillende brandertypes zijn experimenteel getest, hiermee zijn afblaasgradiënten worden bepaald en vergeleken door gebruik te maken van de laminaire afblaastheorie voor niet ontwikkelde stromingen. Verder is een één-staps chemie model ontwikkeld voor een (stoichiometrische) methaan-zuurstof vlam. Een één-staps mechanisms heeft minder rekencapaciteit nodig dan een uitgebreid reactie mechanisme. Het ontwikkelde model komt goed overeen met de vlam eigenschappen voorspeld door grotere mechanismen. Alleen de berekende vlamdikte is een factor 3 kleiner. Deze kleinere vlamdikte vergroot echter de benodigde rekencapaciteit om de vlam numeriek te simuleren, omdat er een fijner rooster nodig is. Om de afblaas snelheid numeriek te bepalen is er gestart met het modelleren van een twee-dimensionale vlam in het computational fluid dynamics pakket *Fluent*.

Verder is gekeken naar nieuwe uitstroom geometriën van branders, waarin de ontwikkeling van een brander met een divergerend kanaal kan worden gezien als een eerste stap in het produceren van een beter presterende brander. Een brander met een divergerend kanaal zorgt voor een lagere snelheidsgradiënt aan de wand. Een divergerend kanaal heeft echt een smaller kanaal nodig alvorens te kunnen divergeren. Dit smallere gedeelte kan gezien worden als een restrictie en als deze restrictie te groot wordt dan kan de stroming niet meer opgevat worden als een incompressible stroming.

Abstract

Oxy-fuel flames are often used in glass heating processes, where high heat-transfer rates are nessesary to obtain a short processing time of the glass. The heat-transfer rate depends on the thickness of the viscous boundary layer at the glass plate; a smaller thickness causes a higher heat flux. To decrease the viscous boundary layer thickness, the strain rate of the burnt gases needs to be increased, which is linearly related to the velocity of the burnt gases. To maximize the burnt gas velocity, the unburnt gas velocity needs to be maximized. The maximum achievable unburnt gas velocity depends on the boundary velocity gradient, which implies that the unburnt gas velocity cannot be raised infinitely, because blow-off of the flame from the burner will occur. The blow-off gradient is, according to theory in literature, not dependent on the diameter of the burner hole. However in the blow-off gradient theory by Lewis and von Elbe [1], the burner shape is never taken into account.

In industry the burner geometry changes in time, due to fouling and wear. This change in geometry influences the flow and thus the blow-off of the flames which in turn relates the blow-off limits to the burner geometry.

In this study, a new insight is gathered in the blow-off criteria of methane-oxygen flames. Several types of burners are tested experimentally and a comparison of the obtained blow-off gradients is made, using the laminar blow-off theory for undeveloped flows.

Furthermore a simple one-step reaction mechanism is developed for a (stoichiometric) methane-oxygen flame. A one-step mechanism circumvents large numerical computations which arise when using a larger reaction mechanism. This one-step mechanism corresponds good to the flame properties as predicted by larger mechanisms, except for the flame thickness which reduces a factor 3. This smaller flame thickness enlarges the computational effort needed to solve the flame numerically, because the need of a finer grid.

To determine the blow-off velocity numerically, a start is made in modeling them two dimensionally by using the computational fluid dynamics (CFD) package *Fluent.*

The development of a burner with a diverging channel can be seen a first step in producing a better performing burner, because simulations of the flow profile show a smaller velocity gradient at the wall. However, a diverging channel obliges the need for a smaller channel before diverging, which results in a restriction in area. When the area restriction is too high, the velocities will raise resulting in a compressible flow.

Contents

Chapter 1

General Introduction

1.1 Background

This master thesis concerns the study of oxy-fuel flames which are often used in the glass forming industry. A typical example of a product made out of glass is a light bulb. There exist a lot of different light bulb shapes; accordingly several process steps are needed to form or cut these bulbs. Most of the bulb shapes are obtained by heating a glass tube locally and in the same time pushing it from both sides. By doing this, the tube will gain in diameter in the area where it is heated. The glass can also be cut by heating it locally. For these processes, very high heat transfer rates are needed.

A major player in the field of light bulbs is Philips Lighting BV. To optimize the processes Philips wants to increase the knowledge about the fundamental processes of heat transfer to glass. To gain this knowledge a cooperation is set up between the Combustion Technology section at the TU/e and Philips Lighting BV in a project called "Pushing the limits of heat transfer by oxy-fuel".

Philips Lighting BV often uses oxy-fuel flames; for these flames oxygen is used as oxidizer instead of air. Oxy-fuel flames have higher temperatures and burning velocities than when air is used as oxidizer, resulting in higher heat fluxes. An other advantage is the possibility to use small burners to heat small surfaces, because of the high burning velocity of oxy-fuel flames.

Research done by Cremers [2] and Remie [3] in this project resulted in a great amount of knowledge about the heat transfer of oxy-fuel flames to glass. Remie showed that the gas velocity after the flame front is almost the same as the unburnt gas velocity and that the heat transfer to the glass product is proportional to the gas velocity. Cremers' thesis concerned the role of chemistry and radiation of the heat transfer. Knowing that the oxy-fuel flame reaches chemical equilibrium before full conversion into products is achieved, one may conclude that the burnt gas stream still has a lot of potential. When the radicals present in the burnt gas flow recombine by a mechanism called Thermo-Chemical Heat Release (TCHR), they can be responsible for up to half of the total heat transfer rate.

This master thesis focuses on the stabilization of premixed laminar stoichiometric oxy-fuel flames on burners to maximize the blow-off velocities, herewith maximizing the heat transfer to the glass product as stated by Remie [3]. Previous research [4, 5] determined the critical blow-off gradients by measuring the blow-off velocities of a deck-plate pot-burner. This study will focus on a special burner used at Philips Lighting BV, known as the Pencil Burner.

1.2 General theory

The advantage of using premixed flames instead of non-premixed flames is the fact that the flame diameter can be kept small, while the fuel and oxidizer flow through the same hole. Therefore several burner holes can be placed near each other to obtain a near homogeneous flow after the flames.
A schematic overview of a premixed laminar flame impinging to glass can be seen in figure 1.1. In this picture the distinguished regions between the burner and the glass are given. In the free jet region, the velocity can considered to be constant.

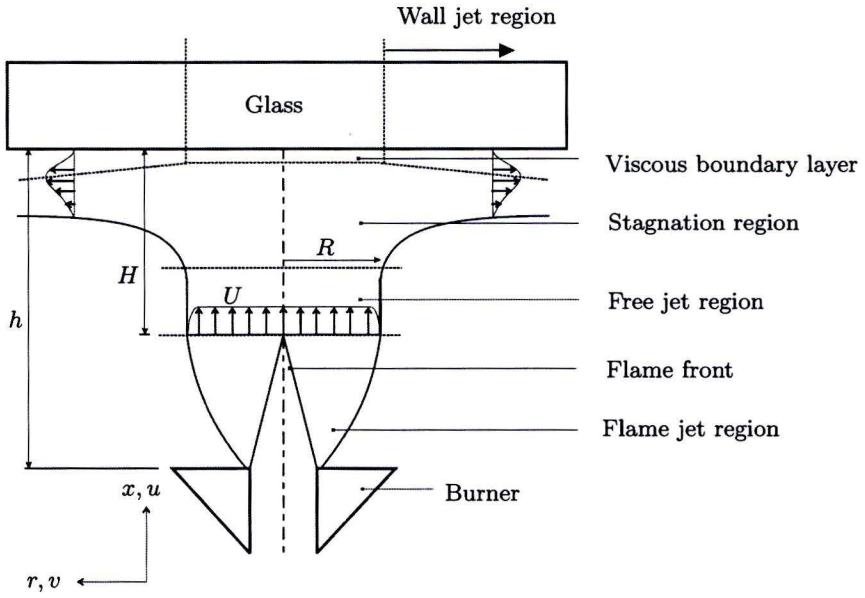

Figure 1.1: Schematic overview of a stagnation flame impinging to a plane surface, adapted from Remie [3]

According to Remie [3] a higher maximum strain rate (a) results in a thinner viscous boundary layer and therefore a higher heat transfer from the burnt gases to the glass product. The strain rate of the burnt gases is the space derivative of the burnt gas velocity (U) and an important factor of the heat flux. In the axisymmetrical case, this maximum strain rate is given by:

$$a = \frac{2U}{H} \quad [1/\text{s}]. \tag{1.1}$$

In equation (1.1) H is the distance between the flame tip and the surface, which can also be seen in figure 1.1. From equation (1.1), it can be concluded that a higher burnt gas velocity increases the maximum strain rate and therefore increases the heat transfer to the glass product. Premixed methane-air flames have a burning velocity of about s_l=0.3 m/s and an adiabatic flame temperature of about T_f=2200 K; premixed methane-oxygen flames have a burning velocity of about s_l=3 m/s and an adiabatic flame temperature of about T_f=3050 K. From the large difference in burning velocity it can be concluded that the maximum strain rate can be much higher when using a methane-oxygen flame and that by using oxygen as oxidizer the heat transfer can be improved significantly.
To increase the heat transfer even more, the achievable burnt gas flow should be maximized.

To raise the velocity of the burnt gas, the velocity of the unburnt gas must be raised. But the velocity of the unburnt gas flow cannot be raised unlimitedly, because the flame will blow off from the burner. Research done by Lewis and von Elbe in 1943 [6] resulted in the "critical gradient theory"which relates the blow-off velocity to the critical blow-off gradient (g_b), and flash-back gradient (g_f).
There are several velocity profiles possible which are shown in figure 1.2. In these pictures the velocity U is given with a dotted line and is assumed to be linear close to the wall. The adiabatic velocity is given by s_l and is zero near the wall due to cooling.

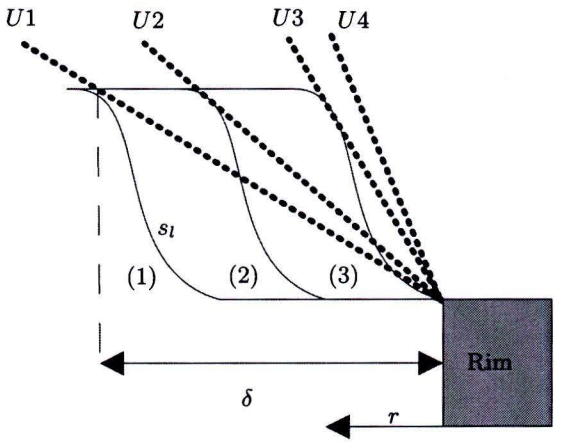

Figure 1.2: Burning velocity and gas velocity; (1) represents the fash-back gradient and (3) the blow-off gradient

In figure 1.2 three situations are shown, where (1) represents the flashback gradient. The flash-back gradient can be written as the adiabatic velocity divided by the stand-off distance (δ): $g_f = s_l/\delta$ [1/s]. The stand-off distance is given as $\delta = \alpha/s_l$ [m], with α the thermal diffusivity in [m^2/s]. Therefore the flash-back gradient scales with the adiabatic flame speed squared, or $g_f \sim s_l^2$. The blow-off gradient is given by position (3), because the flame speed is less then the gas velocity when the gas velocity becomes $U4$. The blow-off gradient is defined as:

$$g_b = \lim_{r \to R} \left(- \frac{dU}{dr} \right), \tag{1.2}$$

where U is the velocity profile [m/s] and r the position on the radius of the burner outlet [m]. For a fully developed poiseuille-flow profile in a round tube, this equation becomes:

$$g_b = \lim_{r \to R} \left(- \frac{dU}{dr} \right) = \frac{4}{\pi} \frac{Q}{R^3} = \frac{4\bar{v}}{R} = \frac{2V_{max}}{R}, \tag{1.3}$$

with Q the flow [m^3/s], $\bar{v}$ the average velocity through the burner hole [m/s] and R the radius of the hole [m].
In 1948 also the blow-off gradients of methane-oxygen flames were presented [7], which are a factor 100 higher than for methane-air flames. This factor can be explained by the relation between the blow-off gradient and the adiabatic flame speed given by the following equation by Reed in 1967 [8] which correlates a lot of experimentally determined stability data:

$$g_b = \frac{0.23 \rho c_p s_l^2}{\lambda} = \frac{0.23 s_l^2}{\alpha}. \tag{1.4}$$

Here is ρ the density [kg/m^3], c_p the specific heat at constant pressure [J/kgK], λ the thermal conductivity [W/mK]. In all the publications mentioned it is shown that the blow-off gradient is not dependent on the burner diameter, however no research was done on the influence of the burner shape.
The dependence of the blow-off gradient on the Reynolds number for a Poiseuille flow is given by Lewis and von Elbe in 1961 [1]:

$$g = fRe\bar{U}/4R, \tag{1.5}$$

where the friction coefficient is:

$$f = 16/Re \quad \text{for } Re < 2000, \tag{1.6}$$

resulting in equation (1.3). For turbulent flows the friction coefficient is:

$$f = 0.046/Re^{0.2} \quad \text{for } 5000 < Re < 200.000, \tag{1.7}$$

which also holds between Re=3000 and Re=5000. The Reynolds number given by:

$$Re \equiv \frac{UL}{\nu}. \tag{1.8}$$

U and L are the characteristic velocity and length respectively, and ν the kinematic viscosity [m^2/s]. Implementing the friction coefficient of equation (1.7) in equation (1.5), this results in:

$$g = \frac{0.023}{\nu^{0.8}} \cdot U^{1.8} \cdot \frac{1}{(2R)^{0.2}} \quad \text{for } 3000 < Re < 200.000. \tag{1.9}$$

In the transition region between Re≈2000 and Re≈3000, an interpolation should be used.

1.3 Problem definition

As described in the previous section, the burner shape is never taken into account in the gradient theory. But observations in practical industry applications at Philips Lighting BV show a changing behavior of the burners in time. Wear of the burner heads due to high temperature and burner fouling (clogging and accumulation) due to quartz vapor, changes the outlet profile of the burner. This change results in burners which do not behave properly and thus fall out. To clean the burners from quartz, a steel brush is used but by doing this the pencils are deformed. To investigate these phenomena it would be very interesting to look closely to the burner nozzle. But because of the high temperatures and velocities of the oxy-fuel flame, it is within the current state of technology almost impossible to obtain a picture of the velocity field near the burner nozzle. Therefore it is difficult to experimentally evaluate the burner-stabilization phenomena.

1.4 Objectives

To solve the problems stated above, the main objective of this research is to obtain more scientific knowledge about the subject of blow-off of oxy-fuel flames. The main research questions which need to be answered are:

- Does the burner shape influence the blow-off velocity and is it possible to define the burner outlet in such a way that the flame attaches longer to the burner, to maximize the blow-off velocities of several burners?

- Is it possible to numerically determine the blow-off velocities using Computational Fluid Dynamics (CFD)?

1.5 Approach

To study the stabilization on the burner outlet/rim into detail, a CFD model is developed using *Fluent*. For this a global one-step kinetic mechanism is made for the methane-oxygen flame using *Chem1D* [9]. To check if the burning behaviour in *Fluent* is the same as the developed one-step model produced using *Chem1D*, a pseudo-1D model is made in *Fluent* and compared with the results of the 1D results from *Chem1D*. To check the numerical results, also experiments on the blow-off velocities need to be done. At first blow-off velocities are determined on a deck-plate burner which was also done by Van Zwieten [4] and Gerth [5]. These results are compared with measured values obtained using new deck plates. The same blow-off velocity measurements are done with the pencil burner which is also used in production processes at Philips Lighting. To study if other burner-outlet shape raise the blow-off velocity, two new pencil burners with different outlet geometries (figures 1.3(b) and 1.3(c)) are designed and for these burners the blow-off velocities are also measured.

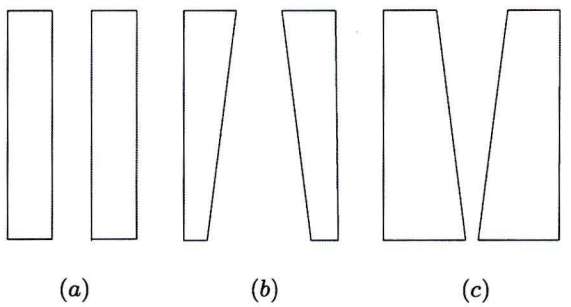

Figure 1.3: Burner channel geometries (a): straight (b): converging (c): diverging

1.6 Outline

To explain which equations are needed to model the laminar premixed combustion the combustion modeling theory will be explained globally in chapter 2. This theory chapter is followed by the simulations in chapter 3 in which the numerical simulation approach is clarified. The development of the new burners and the experiments done with these burners are treated in chapter 4. After this the results of both the simulations and the burner experiments are presented in chapter 5. Chapter 6 discusses the chosen strategy and the results from chapter 5 and is followed by a conclusion in chapter 7. Recommendations concerning this thesis are given in chapter 8.

Chapter 2

Combustion modeling theory

In this chapter a short introduction in laminar premixed combustion is presented. Also, the used models and methods for simulation of flames are described. In the first section 2.1, the combustion and chemistry will be treated and the one-step reaction model will be described. The Physical model, as used in *Fluent*, is described in section 2.2. In this section the conservation equations and the laminar finite rate model are written. To make this section complete the equations for the physical properties, e.g. diffusion coefficients, conductivity and viscosity, are given. The numerical model used in *Fluent* is discussed in section 2.4. The *Chem1d* program and the approximation models are described in section 2.5.

2.1 Combustion and chemistry

Combustion is very complex because of the many reactions happening in a short period of time and space. The main chain through which a methane molecule oxides is given by [10]:

$$CH_4 \rightarrow CH_3 \rightarrow CH_2O \rightarrow CHO \rightarrow CO \rightarrow CO_2, \tag{2.1}$$

where methane (CH_4) is converted to carbon-dioxide (CO_2) via methyl (CH_3), formaldehyde (CH_2O), aldehyde (CHO) and carbon-monoxide (CO). To describe this conversion of methane very precisely, detailed mechanisms are developed. These mechanisms contain a lot of species and reactions. Very well known and commonly used mechanisms are the USA Gas Research Institute (GRI) mechanisms. The last developed mechanism, *GRImech 3.0*, is an optimized mechanism designed to model natural gas combustion, containing 325 reactions and 53 species [11]. A smaller mechanism is the mechanism developed by Smooke [12].
A schematic example of the structure of a premixed flame is shown in figure 2.1.In figure 2.1(a), the flamefront is schematically drawn. In figure 2.1(b) the conversion of the fuel into products can be seen including the formation of intermediates given by the main chain equation (2.1).

2.1.1 One-step reaction

A one-step model can be used to approximate a larger mechanism and thus reduce computational time. A one-step model, which neglects the formation of intermediate species and therefore the entire branched chain of elementary reactions (2.1), can be described by a single overall reaction.

$$\text{Fuel} + \text{Oxidizer} \rightarrow \text{Products} \tag{2.2}$$

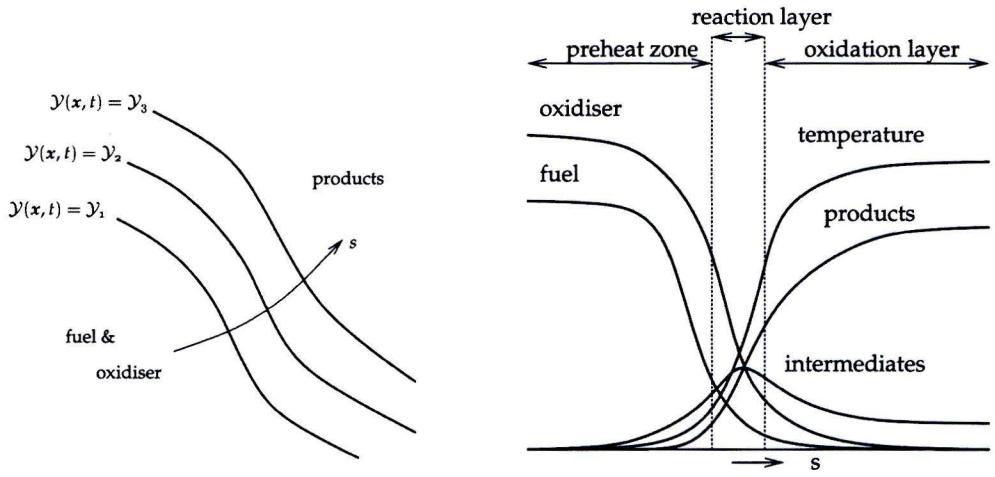

(a) Flamefront (b) Internal flame structure

Figure 2.1: Schematic example of a premixed flame, adapted from Bongers [13]

Former research [10, 14] has shown that a "one-step model"is capable of describing the behavior of the energy transport in the flame reasonably well. Also, it is shown in literature that the global structure of laminar premixed flames is correctly predicted when using a one-step chemical mechanism [15].
If the reaction parameters are chosen appropriately the global reaction in moles of the combustion of pure methane and pure oxygen can be seen in equation (2.3):

$$CH_4 + 2O_2 \rightarrow CO_2 + 2H_2O. \tag{2.3}$$

2.2 The physical model

While *Fluent* is used as the CFD solver, the equations given in this section are the ones used for modeling laminar premixed flames as solved by *Fluent*.

2.2.1 Governing equations

To describe a flame, the model needs to satisfy four conservation equations of mass, momentum, energy and species.
The conservation of mass, also called the continuity equation, is given by:

$$\frac{\partial \rho}{\partial t} + \nabla \cdot (\rho \vec{v}) = 0, \tag{2.4}$$

with the time given by t [s], ρ the density [kg/m^3] and $\vec{v}$ the velocity vector [m/s].
The conservation of momentum is given by:

$$\frac{\partial}{\partial t}(\rho \vec{v}) + \nabla \cdot (\rho \vec{v}\vec{v}) = -\nabla p + \nabla \cdot (\bar{\bar{\tau}}) + \rho \vec{g} + \vec{F}, \tag{2.5}$$

with p the pressure [Pa], $\vec{g}$ the gravitational acceleration vector [m/s^2] and $\vec{F}$ the external body forces. The viscous stress tensor in the momentum equation can be written as:

$$\bar{\bar{\tau}} = \mu\left[(\nabla\vec{v} + \nabla\vec{v}^T) - \frac{2}{3}\nabla\cdot\vec{v}I\right], \tag{2.6}$$

with I the unit tensor [-] and μ the molecular viscosity [kg/ms].
The energy is conserved via:

$$\frac{\partial}{\partial t}(\rho E) + \nabla\cdot(\vec{v}(\rho E + p)) = \nabla\cdot\left(\lambda_{eff}\nabla T - \sum_i h_i\vec{J}_i + (\bar{\bar{\tau}}_{\text{eff}}\cdot\vec{v})\right) + S_h, \tag{2.7}$$

where λ_{eff} [W/mK] is the effective conductivity which is the conductivity plus the turbulent conductivity ($\lambda + \lambda_t$), and the diffusion flux of species i is given by $\vec{J}_i$ [kg/m^{2}s]. The effect of enthalpy transport due to species diffusion is given by $\nabla\cdot(\sum_i h_i\vec{J}_i)$ and the conductivity by $\nabla\cdot(\lambda_{eff}\nabla T)$. The source of energy due to chemical reaction [J/m^{3}s] can be written as:

$$S_h = -\sum_i \frac{h_i^0}{M_{w,i}}R_i, \tag{2.8}$$

where h_i^0 is the formation enthalpy [J/mol], $M_{w,i}$ the molecular mass of species i [kg/mol] and R_i the net source of species i due to chemical reaction [kg/m^{3}s]. The total energy is given by:

$$E = h - \frac{p}{\rho} + \frac{v^2}{2}. \tag{2.9}$$

where h is the sensible enthalpy, which for incompressible flows is defined as:

$$h = \sum_i Y_i h_i + \frac{p}{\rho}, \tag{2.10}$$

with the enthalpy for each species defined as:

$$h_i = \int_{T_{ref}}^{T} c_{p,i}dT. \tag{2.11}$$

When the conservation equation for chemical species needs to be solved, the local mass fraction of each species, Y_i, will be predicted through the solution of a convection-diffusion equation for the i^{th} species. This species conservation equation takes the following general form:

$$\frac{\partial}{\partial t}(\rho Y_i) + \nabla\cdot(\rho\vec{v}Y_i)) = -\nabla\cdot\vec{J}_i + R_i. \tag{2.12}$$

2.2.2 The laminar finite rate model

The laminar finite rate model computes the chemical source terms in equation (2.8) using Arrhenius expressions, and ignores the effects of turbulent fluctuations. The model is exact for laminar flames.

The net source of chemical species i due to reaction, R_i is computed as follows:

$$R_i = M_{w,i} \sum_{r=1}^{N_r} \hat{R}_{i,r} \left[\frac{\text{kg}}{\text{m}^3\text{s}}\right], \tag{2.13}$$

with N_r the number of chemical species in reaction r, and $\hat{R}_{i,r}$ the Arrhenius molar rate of reaction of species i in reaction r [mol/(m^{3}s)].
The reaction rate can be written as:

$$\hat{R}_{i,r} = (\nu''_{i,r} - \nu'_{i,r})\left(k_{f,r} \prod_{j=1}^{N_r} [C_{j,r}]^{\eta'_{j,r}} - k_{b,r} \prod_{j=1}^{N_r} [C_{j,r}]^{\eta''_{j,r}}\right), \tag{2.14}$$

with $\eta'_{j,r}$ and $\eta''_{j,r}$ the forward respectively backward rate exponent for each reactant and product species j in reaction r. The molar concentration of each reactant and product species in reaction r is given by $C_{j,r}$ [mol/m^3]. The stoichiometric coefficients for reactant or product i in reaction r are given by $\nu'_{i,r}$ and $\nu''_{i,r}$ respectively. While all reactions used in this thesis are irreversible, the backward rate constant $k_{b,r}$ is zero. The forward rate constant for reaction r is computed using following Arrhenius expression:

$$k_{f,r} = A_r T^{\beta_r} \text{e}^{-\text{E}_\text{r}/\text{RT}}, \tag{2.15}$$

where A_r is the pre-exponential factor [consistent units], β_r the temperature exponent [-] and E_r the activation energy for the reaction [J/mol]. The activation energy divided by the Universal gas constant $R = 8.314$ [J/mol K] gives the activation temperature $T_A = E_r/R$ [K].

2.3 Physical properties

2.3.1 Mass diffusion

Mass diffusion coefficients are required whenever species transport equations in multi-component flows are solved. Mass diffusion coefficients are used to compute the diffusive flux of chemical species in a laminar flow. The diffusion velocity of species i, $\vec{V}_i = \vec{J}_i/\rho$, is determined by pressure gradients, concentration gradients of the species, temperature gradients (Soret effect) and differences in external forces [14]. In the case of combustion with air, nitrogen is the abundant component, and V_i may be assumed to be proportional with the gradient of species i, leading to Fick's Law. In laminar atmospheric combustion processes the diffusion due to pressure gradients, external forces and temperature gradients is small [14, 16], and can therefore be neglected.
The mass diffusion can be computed on two ways. The easiest method is to use Fick's Law. The second is to use the Full Multi-Component method, which in turn uses the Maxwell-Stefan equations.

Fickian diffusion

This diffusion can be defined by the Fick's first law of diffusion, in terms of mass diffusion:

$$\vec{J}_i = -\rho D_{i,m} \nabla Y_i - D_{T,i} \frac{\nabla T}{T}, \tag{2.16}$$

where $D_{i,m}$ is the mass diffusion coefficient for species i in the mixture m [m^2/s] and $D_{T,i}$ the Thermal (Soret) diffusion coefficient [m^2/s].

Equation (2.16) is strictly valid when the mixture composition is not changing, or when $D_{i,m}$ is independent of composition. This is an acceptable approximation in dilute mixtures when $Y_i << 1$, for all i except the carrier gas (in this case N_2).

The mass diffusion coefficient for species i in the mixture can be determined in two several ways. By using the equation (2.17) below or by using constant Lewis numbers.

Mass diffusion coefficients

$$D_{i,m} = \frac{1 - X_i}{\sum_{j,j\neq 1}(X_j/\mathcal{D}_{i,j})}, \tag{2.17}$$

where X_i is the molar fraction of species i [-]. In equation (2.17), the mass diffusion coefficients are calculated using the binary diffusion coefficients of species i in species j, $\mathcal{D}_{i,j}$. Values for $\mathcal{D}_{i,j}$ can be defined if known from literature or calculated using kinetic theory of gases via equation 2.18.

Binary diffusion coefficients using Kinetic theory

The solver used in *Fluent* is able to calculate the binary diffusion coefficients $\mathcal{D}_{i,j}$, using modification of the Chapman-Enskog formula [17]. This determination of the binary diffusion coefficients is based on kinetic theory, and can only be used when the ideal gas law is used. The mass diffusion coefficients, $\mathcal{D}_{i,j}$ is predictable within about 5% using the kinetic theory for binary mixtures of non-polar gases [18]:

$$\mathcal{D}_{i,j} = 0.0188\frac{[T^3(\frac{1}{M_{w,i}} + \frac{1}{M_{w,j}})]^{1/2}}{p_{abs}\sigma_{ij}^2\Omega_D}, \tag{2.18}$$

where p_{abs} is the absolute pressure, and k_B the Boltzmann constant. The Lennard-Jones parameters are the L-J characteristic Length, σ_i, given in angstrøm (Å) and the L-J energy parameter, $(\epsilon/k_B)_i$, in absolute temperature [19]. The diffusion collision integral Ω_D is a function of T_D^*:

$$T_D = \frac{T}{(\epsilon/k_B)_{ij}}, \tag{2.19}$$

$$(\epsilon/k_B)_{ij} = \sqrt{(\epsilon/k_B)_i(\epsilon/k_B)_j}. \tag{2.20}$$

Mass diffusion coefficients using Constant Lewis

An approximation of the mass diffusion coefficients in a mixture can be made using the so called constant Lewis approach. The Lewis number is defined as follows:

$$Le \equiv \frac{\lambda}{\rho c_p D_{i,m}} = \frac{\alpha}{D_{i,m}} = \frac{\text{rate of energy transport}}{\text{rate of mass transport}}. \tag{2.21}$$

Full multi component diffusion

In diffusion-dominated laminar flows, details of the molecular transport processes are significant. Therefore a careful treatment of chemical species diffusion in the species transport and energy equations is important. This can be done using the Full Multicomponent Diffusion (FMD) model. The FMD model uses the Maxwell-Stefan equations:

$$\sum_{\substack{j=1 \\ j\neq i}}^{N} \frac{X_i X_j}{\mathcal{D}_{i,j}}(\vec{V}_j - \vec{V}_i) = \vec{d}_i - \frac{\nabla T}{T}\sum_{\substack{j=1 \\ j\neq i}}^{N} \frac{X_i X_j}{\mathcal{D}_{i,j}}\left(\frac{D_{T,j}}{\rho_j} - \frac{D_{T,i}}{\rho_i}\right), \tag{2.22}$$

in where $\vec{V}_i = \vec{J}_i/\rho$ and if the external force is assumed to be the same on all species and that pressure diffusion is negligible, then $\vec{d}_i = \nabla X_i$. After matrix inversion, the following formulation for the diffusive mass flux vector is obtained:

$$\vec{J}_i = -\sum_{j=1}^{N-1} \rho D_{ij} \nabla Y_j - D_{T,i}\frac{\nabla T}{T}, \tag{2.23}$$

where D_{ij} is a matrix of (N-1)x(N-1) containing the the generalized Fick's law diffusion coeffients $\mathcal{D}_{i,j}$ derived via equation 2.18.

2.3.2 Thermal diffusion

Thermal diffusion (Soret) tends to drive light species towards the hotter parts and heavy species towards colder parts of the mixture [20]. Dufour is the counterpart of the Soret diffusion.

The thermal diffusivity is closely related to the molecular mass. A lower molecular mass results in a higher thermal diffusivity. When the thermal diffusion is higher, s_l is higher as well [18]. This is also shown by Bongers [13].

The thermal diffusion coefficients are defined using the following empirically-based composition-dependent expression:

$$D_{T,i} = -2.59 \cdot 10^{-7} T^{0.659}\left[\frac{M_{w,i}^{0.511} X_i}{\sum_{i=1}^{N} M_{w,i}^{0.511} X_i} - Y_i\right] \cdot \left[\frac{\sum_{i=1}^{N} M_{w,i}^{0.511} X_i}{\sum_{i=1}^{N} M_{w,i}^{0.489} X_i} - Y_i\right]. \tag{2.24}$$

2.3.3 Viscosity

The viscosity can be given as a constant, as a function of time, or can be computed using the kinetic theory:

$$\mu = 2.67 \cdot 10^{-6} \frac{\sqrt{M_w T}}{\sigma^2 \Omega_\mu}. \tag{2.25}$$

From this equation it can be seen that the viscosity depends on the molecular mass and the temperature. It is very important to take this into account because the temperature raises a factor of 10 over the flamefront, and the flow properties highly depend on it, e.g. the transition from laminar to a turbulent flame.

2.3.4 Thermal conductivity

The thermal conductivity can be computed using the kinetic theory:

$$\lambda_i = \frac{15}{4}\frac{R}{M_w}\mu\left[\frac{4}{15}\frac{c_p M_w}{R} + \frac{1}{3}\right]. \tag{2.26}$$

Using the ideal gas mixing law (IGML):

$$\lambda = \sum_i \frac{X_i \lambda_i}{\sum_j x_j \phi_{ij}}, \tag{2.27}$$

$$\phi_{ij} = \frac{[1 + (\frac{\mu_i}{\mu_j})^{1/2}(\frac{M_{w,i}}{M_{w,j}})^{1/4}}{[8(1 + \frac{M_{w,i}}{M_{w,j}})]^{1/2}}. \tag{2.28}$$

Thermal diffusion can be neglected when air is used as oxidizer, but when oxygen is used, neglecting the thermal diffusion leads to an error in the estimation of the burning velocity [21].

2.4 The numerical model

Fluent contains two numerical method solvers, a segregated and a coupled solver. The coupled solver solves the governing equations simultaneously, while the segregated solver solves them sequentially, first the momentum, than the continuity and at last the energy equation. The segregated solver is developed for incompressible flows, while the coupled solver was originally designed for compressible flows. The coupled solver could have an advantage when solving very fine meshes [22].

In both cases *Fluent* uses control-volume-based technique: to divide the the domain into discrete volumes using a computational grid, to integrate the governing equations on the control volumes to construct algebraic equations of the discrete depended variables, to linearize the discrete equations and solve the resulting linear equations to yield the updated values of the dependent variables.

Both numerical methods have the similar finite volume method (FVM) discretization process, but the used approach to linearize and solve the discrete equations is different for both.

Chemical kinetics cause the system of differential equations to be very stiff. Physically, stiffness corresponds to a process whose components have highly disparate time scales or a process whose time scale is very short compared to the interval over which it is being studied. Due to this stiffness it is inevitable to use expensive implicit solvers [23]. The advantage of using an implicit solver is the faster convergence due to a greater stability of the implicit step allowing larger and thus less steps [24].

Solving implicit means that the linearization is done implicit which mean that, for a given variable, the unknown value in each cell is computed using a relation that includes both existing and unknown values from neighboring cells. Therefore each unknown will appear in more than one equation in the system, and these equations must be solved simultaneously to give the unknown quantities [22].

2.4.1 Mesh generation

Numerical modeling of two-dimensional laminar flames on relatively large burners ($O(10^{-2})$m) has one major difficulty, which is the large difference in typical length scales between the burner size and the grid spacing. This is needed to solve the processes inside the flamefront, which, in case of a methane-oxygen flame, has a thickness of the order $O(10^{-4})$m. In order to get reliable results, the amount of cells on the flamefront should be in the order of 10. This means the cell size should be in the order of $O(10^{-5})$m or smaller.
There are several mesh shapes that can be used. An equidistant grid has a constant distance between the cells, while a non-equidistant grid has different distances between the cells. The shape of the cells can be quadratic or triangular or a combination of both.
It is possible to adapt the grid for local refinement of the mesh near regions with high strain rates. Then *Fluent* can use the hanging node adaption. In this procedure an extra point is added to the cell, in between the corner points. It is in this way possible to make 4 cells out of one. The hanging node value is interpolated from the existing two points.
When using the hanging node adaption, coarsening the grid is limited to the original grid. The problem of using one of the local refinement techniques is that the refinement needs a reasonably well converged solution. Otherwise, refinement will be done in the wrong regions of the domain.

2.5 *Chem1D*

Chem1D is an 1D combustion solver developed in the combustion section at the University of Technology Eindhoven (TU/e) [9].
In this solver several burner types like a counterflow or a burner stabilized burner can be modeled, in order to calculate the important flame characterizations. By using this solver, it is possible to compare the behavior of different combustion mechanisms like *GRImech*.
When the adiabatic flame model is used, the grid is fixed to a specific temperature at one point in the domain, and the grid will be refined on this position.
In *Chem1D* some approximation models are programmed. It is possible to use constant or unit Lewis numbers for the calculation of the diffusion.

2.5.1 Constant or unit Lewis numbers

The first approximation is the assumption that the ratio between diffusive transport of heat and the diffusive fluxes of species is constant, i.e. the Lewis numbers are constant. In an even more simplified model, the Lewis numbers are equal to one, $Le_i = 1$. In *Chem1D* the thermal diffusion (D_i^T) is not taken into account when the constant Lewis approach is used.

2.5.2 c_p-relations

When using the constant or unit Lewis numbers approach, *Chem1D* uses two c_p-relations. The conductivity and the specific heat are linked via a relation which was first derived by Smooke and Giovangigli [12]. This relation is given in equation 2.29.

$$\frac{\lambda}{c_p} = B_c \left(\frac{T}{298.0} \right)^{n_c}, \tag{2.29}$$

where the proportionality constants for a stoichiometric methane/air flame under atmospheric conditions are: $B_c = 2.58 \cdot 10^{-4}$ and $n_c = 0.7$

The viscosity and the specific heat are linked via equation 2.30.

$$\frac{\mu}{c_p} = B_v \left(\frac{T}{298.0} \right)^{n_v}, \tag{2.30}$$

where the proportionality constants for a stoichiometric methane/air flame are: $B_v = 1.67 \cdot 10^{-4}$ and $n_v = 0.51$.

Chapter 3

Numerical Simulations

To observe the blow-off of flames, the flames should be modeled at least two-dimensional, which is done using the CFD package *Fluent*. In this research project it is chosen not to use detailed chemistry for the simulation of flames. The main reason for this is to reduce the computational effort needed to model the flames. We are only interested in the stabilization of flames, therefore we are not specially interested in the specific species production. Consequently a one-step model might be a good choice. To determine the parameters for the one-step mechanism, *Chem1D* is used. Thereafter the developed one-step mechanism is implemented in *Fluent*.
This chapter is divided in two main sections. First, the simulations performed in *Chem1D*, including the development of the one-step mechanism, will be treated. In the second section the validation of the one-step mechanism is described and the flame simulations executed in *Fluent* will be shown as well.

3.1 *Chem1D*

In chapter 2, the principle of *Chem1D* is explained. In this section the development of the one-step kinetic mechanism for the methane-oxygen flame will be explained. When developing a one-step model to substitute a large complex combustion mechanism, some assumptions need to be made, which will also be explained.

3.1.1 One-step mechanism development

To develop a one-step mechanism with flame properties corresponding to the properties of a larger mechanism like *GRI 2.11* or *Smooke*, the model should be adjusted to fit the essential combustion properties such as the adiabatic flame temperature (T_{ad}) and the adiabatic flame velocity (s_l). The approximation of one (global) reaction for the burning of methane with oxygen is a rather big one. In reality a methane-oxygen flame creates a lot of compounds like hydrogen (H_2), hydroxide (OH) and oxygen (O) and produces also considerable amounts of carbon monoxide (CO). When removing these species from the combustion mechanism, the adiabatic flame temperature will rise to non-physical heights. The compounds mentioned above, which are present in the real burnt gases have a high formation enthalpy and the formation enthalpy of carbon monoxide is less negative than of carbon dioxide. When the enthalpy change from the compounds and carbon monoxide is neglected, the total enthalpy will be higher. This results in a high adiabatic temperature corresponding to equation (2.11). The predicted adiabatic temperature without the

mentioned compounds and CO is about 5000 K, while the adiabatic flame temperature is about 3050 K in real life.
There is only one method to temper the adiabatic flame temperature when these radicals and CO are not taken into account in the reaction mechanism, which is increasing the specific heat at constant pressure (c_p). Normally, the specific heat increases with temperature. For the model in this study the specific heat is chosen to have a constant value, because this can be more easily determined empirically. When the specific heat is changed, the factors in the c_p-relations in equations (2.29) and (2.30) should also be changed, otherwise a wrong estimation of the viscosity and conduction would be made. The new determined values of the proportionality constants of the c_p-relations are given in table 3.1.
The diffusion is chosen to be represented by Lewis=1, thus assuming the mass diffusion equal to the thermal diffusivity. This approximation can be justified because there is only one global reaction and the other parameters are fitted to obtain the correct flame speed.
Bongers showed in his thesis that when the thermal diffusion (Soret diffusion) is taken into account, the adiabatic burning velocity (s_l) is slightly reduced for a methane-oxygen flame [13]. This deviation is accounted for by fitting, as will be described below, and therefore the thermal diffusion is not modeled.

Determining the mechanism parameters

The one-step model can be fitted to a detailed by adjusting the reaction rate, as described with equation (2.13). For the one-step methane-oxygen fuel, the reaction is considered to be irreversible, and therefore the backward rate constant is zero, leaving only the forward rate constant (k_f). For the one-step mechanism for methane-oxygen, which is given in equation (2.3), the reaction rate equation, given by (2.14), can be reduced and written as:

$$\hat{R} = (\nu''_{i,r} - \nu'_{i,r})\left(k_f[C_{CH_4}]^{\eta'_{CH_4}}[C_{O_2}]^{\eta'_{O_2}}\right), \tag{3.1}$$

where η'_{CH_4} and η'_{O_2} are rate exponents for methane and oxygen concentrations (C_{CH_4},C_{O_2}) respectively, which are chosen arbitrarily and have the same value as the stoichiometric coefficients ν_{CH_4} and ν_{O_2}. The other two parameters to fit the flame properties, the activation temperature (T_A) and pre-exponential factor (A_r), are combined in the forward rate, as given by equation (2.15). The activation temperature will be calculated from burner-stabilized flames and the pre-exponential factor will be estimated.
To obtain a one-step model which describes the dependence on heat-loss accurately, the correct activation temperature (T_A) needs to be found by performing some numerical calculations of a burner stabilized flame. This is done by using the burner stabilized model in *Chem1D* with the *Smooke* mechanism. When the inlet velocity (U) is below the flame speed (s_l), heat will be transferred to the burner and thus lowering the flame temperature (T_f). The flame temperatures are calculated for several different inlet velocities. When the logarithm of de inlet velocity is plotted against the inverse of the flame temperature, see figure 3.1. The slope of the line fit through these data points represents (-$2T_A$) because the flame speed is related to $s_l \sim e^{-T_A/2T}$. This relation arises from the formulation of the Arrhenius expression in the forward reaction rate, given by equation (2.15) and the. The flame temperature will be equal to the adiabatic temperature (T_{ad}) when the inlet velocity is equal to the adiabatic flame speed, depicted by the circle in figure 3.1.
After the determination of the activation temperature, the specific heat has to be determined empirically to get the same adiabatic flame temperature as for the *Smooke* mechanism. After this, the pre-exponential factor is tuned to obtain the same adiabatic flame speed as predicted by

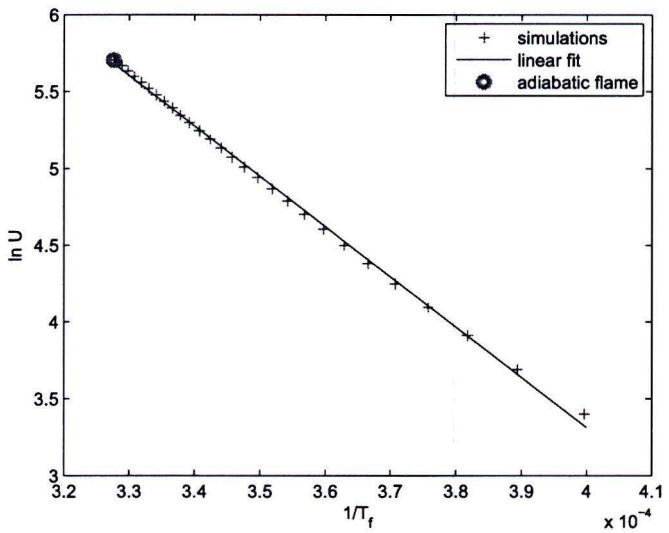

Figure 3.1: Determination of T_a using the burnerstabilized model, the green circle represents the $\ln s_l - T_b$ point.

the simulations with the *Smooke* mechanism. The determined mechanism parameters are given in table 3.1.

Table 3.1: One-step mechanism parameters for CH4/O2 at ϕ=1.0 using *CHEM1D*

c_p	specific heat	3635 J/(kgK)
η'_{CH_4}	forward rate constant for methane	1
η'_{O_2}	forward rate constant for oxygen	2
T_A	activation temperature	16734 K
A_r	pre-exponential factor	$3.2 \cdot 10^{21}$ $(\text{mol/cm}^3)^{-2} \cdot s^{-1}$
B_v	constant in the $\mu - c_p$ relation	$4.79 \cdot 10^{-5}$
n_v	exponent in the $\mu - c_p$ relation	0.72
B_c	constant in the $\lambda - c_p$ relation	$8.38 \cdot 10^{-5}$
n_c	exponent in the $\lambda - c_p$ relation	0.96

Table 3.2: Mechanism properties for CH4/O2 at ϕ=1.0 from *CHEM1D*

	GRI2.11	Smooke	1 step
s_l [m/s]	3.036	3.06	3.045
T [K]	3115	3052	3053
$\dot{m}$ [gr/(cm^{2}s)]	$3.314 \cdot 10^{-1}$	$3.3395 \cdot 10^{-1}$	$3.30 \cdot 10^{-1}$
δ_f [m]	$8.955 \cdot 10^{-5}$	$9.078 \cdot 10^{-5}$	$2.97 \cdot 10^{-5}$

In table 3.2 it is shown that the flame thickness (δ_f), the distance between the two points with the highest gradient of the Arrhenius rate of reaction, of the one-step model is about 1/3 the value when comparing to advanced mechanisms. This is a negative effect of adapting the specific

heat to fit the required adiabatic temperature. The specific heat is approximately two times higher than the specific heat for the correct burnt gases at 3000 K (c_p ≈2300 J/(kgK)) and almost three times higher at 300 K (c_p ≈1200 J/(kgK)). The dependence of the laminar flame speed on the thermal diffusivity and the reaction rate is given by equation 3.2, which is first derived by Mallard and LeChatelier and rewritten in Kuo [18]:

$$s_l \propto \sqrt{\alpha \cdot RR} \tag{3.2}$$

From equation (3.2) it can be concluded that when the specific heat (c_p) is larger, the reaction rate (RR) should also be larger to obtain the same flame velocity. According to equation (3.3), the flame thickness will then be smaller:

$$\delta_f \propto s_l \frac{1}{RR}. \tag{3.3}$$

3.2 *Fluent*

To check the flame properties given by *Chem1D*, a pseudo one-dimensional model is built in *Fluent*. This test case is used to compare the one-step model for methane-air, which is taken from the *Fluent* library, and the new developed one-step model for methane-oxygen. After both test cases, the outflow profile of the burners is determined, by simulating the channels in *Fluent*. The flow profiles are given in section 3.2.2, followed by the simulations of the 2D flames in section 3.2.3.

3.2.1 One-step 1D validation test case

The adiabatic temperature and flame velocity results from *Chem1D* are validated in *Fluent* using a pseudo one dimensional model which is schematically shown in figure 3.2. The model has a height (H) of only one cell. The modeling domain is symmetrical, and due to this boundary condition there is no gradient between the top and bottom side of the domain. The model is initiated by setting the unburnt gas properties on the left side of the domain (1), and the burnt gas properties on the right side of the domain (2). At the end an outflow or a pressure outlet is defined and in the front, at the beginning of the domain, a velocity inlet (v_{in}) is defined.

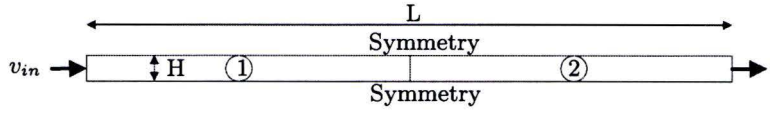

Figure 3.2: Domain of the one-step 1D validation test case

Checking the adiabatic flow velocity is done by performing time-dependent (unsteady) calculations. The inlet velocity (v_{in}) is chosen to be smaller than the adiabatic flow velocity from the *Chem1D* calculations. Hereby, the flame will travel through the domain to the left, see figure 3.3. By measuring the position of the top of the reaction rate on several points, the travel velocity can be calculated by using $v_{travel} = d/t$. Adding the travel velocity with the chosen inlet velocity results in the adiabatic flame velocity ($s_l = v_{in} + v_{travel}$).

Methane-air flame

In this section the results of the pseudo 1D simulations of the methane-air flame are discussed. The parameters of the one-step model from the *Fluent* library are given in table 3.3. When

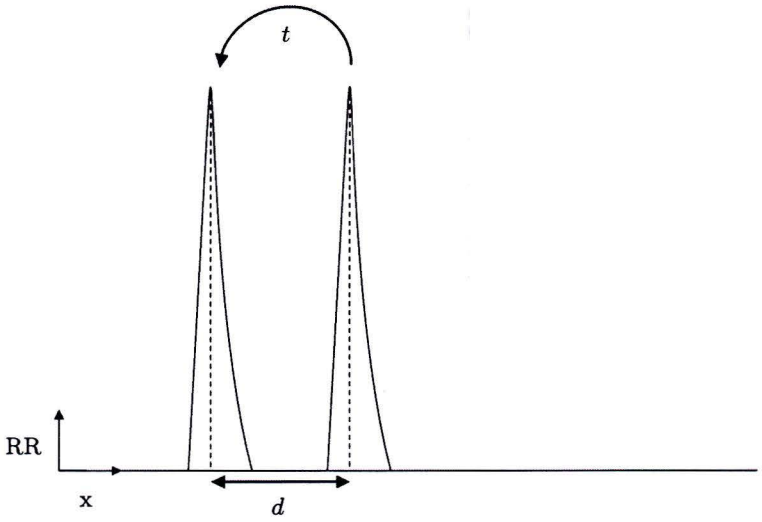

Figure 3.3: Reaction Rate peaks of one-step 1D validation test case

simulating this flame in *Chem1D*, using the constant Lewis numbers given in appendix A, the predicted burning velocity is s_l=22.06 cm/s.

Table 3.3: One-step parameters from the *Fluent* library for CH4/air

η'_{CH_4}	forward rate constant for methane	0.2
η'_{O_2}	forward rate constant for oxygen	1.3
T_A	activation temperature	24380 K
A_r	pre-exponential factor	$6.7 \cdot 10^{12}$ $(mol/cm^3)^{-0.5} * s^{-1}$

Several pseudo-1D simulations are done in *Fluent* with different models and approximations. The simulations and results are summarized in table 3.4. In this table the following abbreviations are used;

- ID is the inlet diffusion, this is used (Y) or not (N).
- KT means kinetic theory as described in section 2.3.
- ML is the mixing law used for the determination of the specific heat $c_p = \sum_i Y_i c_{p,i}$.
- IGML the ideal gas mixing law, which for the thermal conductivity is given by equation (2.27). The IGML has the same form for the viscosity.
- DA is dilute approximation , see section 2.3.1.
- Fick means that the Fickian diffusion model is used.
- FMD stands for full multi component diffusion using kinetic theory.
- C1D means that the values used are described by a polynomial derived from *Chem1D* cases.

Table 3.4: One-step validation for CH_4/air at ϕ=1.0 on pseudo 1D grid with gridsize of $2.5 \cdot 10^{-4}$ mm

	ID	Mass diff.	c_p [j/(kgK)]	λ [W/(mK)]	s_l [cm/s]
1	Y	KT : FMD	ML :GRI	IGML: KT	19.38
2	Y	KT: Fick	ML :GRI	IGML: KT	19.13
3	Y	KT: FMD	ML:FLUENT	IGML: KT	18.88
4	Y	KT: Fick	ML:FLUENT	IGML: KT	19.25
5	N	KT: Fick	ML:FLUENT	IGML: KT	19.5
6	Y	DA:C1D	ML:FLUENT	IGML: KT	19.75
7	Y	DA:C1D	ML :GRI	IGML: KT	19.75
8	Y	DA:C1D	ML :GRI	C1D	22.25
9	Y	DA:C1D	C1D	C1D	21.35
10	N	DA:C1D	C1D	C1D	22.13
11	Y	KT: FMD	C1D	C1D	21.25
12	N	KT: FMD	C1D	C1D	21.50
13	Y	KT: Fick	ML :GRI	C1D	21.67

The viscosity used is calculated using IGML:KT, the diffusion as energy source is taken into account and the thermal diffusion is neglected. The inlet velocity is v_{in}=0.1 cm/s.
From table 3.4 several conclusions can be drawn.

- Inlet diffusion
  When comparing the results of case 4 with 5, case 9 with 10 and case 11 with 12, one can conclude that taking the inlet diffusion into account results in a lower flame speed. However, this effect will only be seen when the flame front is close to the inlet, which is true for these test cases. The maximum difference is 3.5%.

- Mass diffusion
  When comparing the results of case 1 with 2 and 7, case 3 with 4 and 6 and case 9 with 11, one may conclude the chosen diffusion model does have a slight influence. The dilute approximation from the constant Lewis numbers results in the highest flame speed. The biggest difference is around 4 %.

- Specific heat
  When comparing the results of case 1 with 3, case 2 with 4 and case 6 with 7, one may conclude that the difference between the c_p polynomials of *GRI* and *Fluent* is almost zero, the highest difference is around 2,5%. But the polynomials from the *chem1D* model result in a lower s_l compared to the *GRI* polynomials, here the difference is about 4%.

- Conductivity
  The highest influence on the burning velocity is given by the calculation of the conductivity. Comparing case 7 with 8 and case 2 with 13, it is possible to conclude that the derived polynomials from the *chem1D* calculations push the burning velocities to a higher level by about 12%.

The results in table 3.4 are compared with the flame speed of s_l=22.06 cm/s. From this can be concluded that, when using the polynomials derived from *Chem1D*, the results of case 9 and 10, are almost the same as predicted by *Chem1D*. When taking the inlet diffusion into account, the difference is about 3%. When neglecting inlet diffusion, which is also done by *Chem1D*, the difference is about 0.3 % on this grid size of $2.5 \cdot 10^{-4}$ m.

Methane-oxygen flame

The assumptions made in the development of the one-step mechanism should also be used in the simulations in *Fluent*. This is done by describing the physical properties, calculated by *Chem1D*, by polynomials of each parameter depending on the temperature. The polynomials for the diffusion coefficients, $D_{i,m}$, are determined by using equation (2.21), where the polynomial of the thermal diffusivity (α) is divided by the Lewis number of the species. While the diffusion is approximated by unit Lewis numbers for all species, the polynomials describing the diffusion coefficients are equal to α for all species.

Also the conduction coefficient (λ) and dynamic viscosity (μ) as a function of temperature are derived from the *Chem1D* calculations and used as input in *Fluent*. The polynomials can be found in appendix A. In *Fluent* the thermal diffusion is neglected, because this is also neglected during the development of the one-step mechanism.

For the methane-oxygen flame the grid dependence on the flame-speed is investigated. For the domain, a channel length of L=2 cm is chosen and an inlet velocity of v_{in}=1 m/s with different cell sizes. For the simulation of this flame, only the polynomials from the *Chem1D* simulations are used as input. The polynomials can be found in appendix A. The results of the test cases are shown in table 3.5. When comparing cases 1,2,3 and 6 shown that the grid size has a considerable dependence on the computed flame speed. The flame speed computed in *Fluent* will become equal to the *Chem1D* prediction when the grid size is smaller than $1.25 \cdot 10^{-6}$ m. The time steps should be chosen smaller when a smaller grid is simulated, otherwise non-physical pressures will be calculated.

Table 3.5: One-step validation for CH4/O2 at ϕ=1.0 on pseudo 1D grid, using the segregated

Case number	1	2	3	4	5	6
Upwind scheme	1st	1st	1st	2nd	2nd	1st
Inlet diffusion	y	y	y	y	n	y
Cell size [m]	$1 \cdot 10^{-5}$	$5 \cdot 10^{-6}$	$2.5 \cdot 10^{-6}$	$2.5 \cdot 10^{-6}$	$2.5 \cdot 10^{-6}$	$1.25 \cdot 10^{-6}$
Time step [s]	$1 \cdot 10^{-7}$	$1 \cdot 10^{-7}$	$1 \cdot 10^{-8}$	$1 \cdot 10^{-8}$	$1 \cdot 10^{-8}$	$1 \cdot 10^{-9}$
Reaction rate [kmol/(m^{3}s)]	$1.40 \cdot 10^3$	$1.58 \cdot 10^3$	$1.67 \cdot 10^3$	$1.66 \cdot 10^3$	$1.65 \cdot 10^3$	$1.69 \cdot 10^3$
s_l [m/s]	3.48	3.33	3.18	3.05	3.03	3.06

From table 3.5 can be concluded that when refining the grid, the reaction rate is predicted better, the reaction rate predicted by *Chem1D* is $1.69 \cdot 10^3$ kmol/(m^{3}s). From these results it can be concluded that when the grid size is smaller, the predicted flame speed approaches the flame speed as predicted by *Chem1D*. Using the 2nd order scheme, the flame speed lowered. Neglecting inlet diffusion combined with a second order upwind scheme underpredicts the flame speed on a grid with a cell size of $2.5 \cdot 10^{-6}$ m.

3.2.2 Flow profiles

Since the blow-off gradient is given by the spatial derivative of the flow velocity at $r = R$, it is very important to know the outflow velocity profile. The velocity gradient of a plug flow or a non-developed Poiseuille flow, is much higher than a developed Poiseuille flow profile. The derivation of the blow-off gradient can be found in appendix C, and is given by:

$$g_b = \lim_{r \to R} \left(-\frac{dv}{dr} \right) = \frac{1 + \alpha_p}{\alpha_p} \frac{1}{R} V_{max}, \tag{3.4}$$

where α_p is the factor of the development of the flow corresponding to the developed Poiseuille profile and which is given by:

$$\alpha_p = \frac{\frac{V_{max}}{\bar{v}} - 1}{3 - \frac{V_{max}}{\bar{v}}}. \tag{3.5}$$

When the profile is a completely developed Poiseuille profile, then α_p=1. To determine the velocity profile at the outlet of each burner as function of the radius and mean velocity, burners with different internal channel geometries are modeled in *Fluent* assuming a no-slip condition at the wall. The viscosity used is the one of a stoichiometric methane-oxygen mixture at 300 K, calculated using the polynomial given in appendix A.

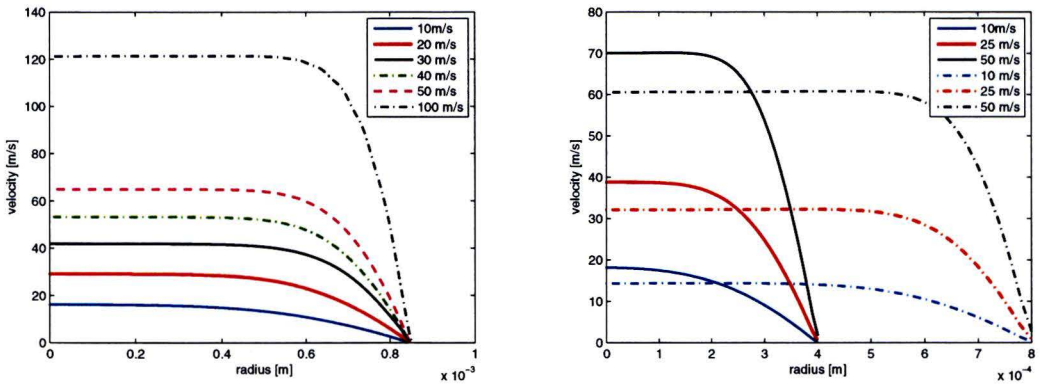

(a) Steel, straight channel, Philips pencil burner

(b) Deck-plate burners

Figure 3.4: Axial velocity flow profiles

In figure 3.2.2 a comparison is made between the obtained flow profile using *fluent* and formula C.3 with $\alpha = 0.12$ derived via equation 3.5. From this can be concluded that the derived equation for describing the undeveloped velocity profile described the profile good.
Figure 3.4(a) shows the velocity profiles of a straight channel burner, while the properties of the flow profiles compared to a developed Poiseuille flow are written in table 3.6. From table 3.6 it can be concluded that velocity gradient at $r = R$, g, for the non-developed flow is much higher than the velocity gradient of a developed Poiseuille flow g_p. For an average velocity of 100 m/s the gradient of a non-developed flow is 2.85 times higher than of a developed Poiseuille profile. This means that for a specific blow-off gradient limit, the non-developed flow will blow-off earlier. From these simulations it can be concluded that, the internal burner geometry of the original pencil is not the best for these high velocities, because the fully developed profile is not obtained. The flow-profiles of the deck plate burners are depicted in figure 3.4(b)and the properties are

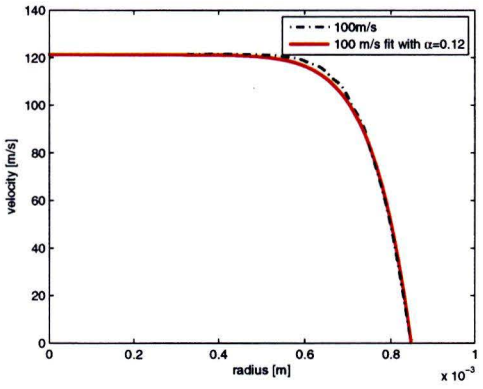

Figure 3.5: Axial velocity flow profile; comparison of the obtained flow profile from Fluent with the fit by equation C.1

Table 3.6: Flow development of the steel, straight channel, Philips pencil burner

$\bar{v}$ [m/s]	10	20	30	40	50	100
V_{max} [m/s]	16.2	29.2	41.8	53.2	65	121.3
$V_{max,p}$ [m/s]	20	40	60	80	100	200
V_{max}/V [m/s]	1.62	1.46	1.39	1.33	1.30	1.21
α_p	0.45	0.30	0.24	0.20	0.18	0.12
g/g_p	1.30	1.61	1.81	2.00	2.15	2.85

written in table 3.7. When comparing table 3.6 and table 3.7 for a mean velocity of 50 m/s it can be concluded that the velocity gradient of the R=0.4 mm deck plate is lower and of the R=0.8 mm deck plate is higher then the velocity gradient of the straight steel pencil. This is due to the length of the channel, which is 25 times the diameter for the R=0.4 mm burner, about 20 times the diameter for the straight steel pencil and 12.5 times the diameter for R=0.8 mm.

The velocity profiles of the converging pencil depicted in figure 3.6(a) are even steeper than the undeveloped flow of the steel, straight channel, Philips pencil burner. This will result in higher blow-off gradients at lower velocities and thus a lower blow-off velocity.

The velocity profiles at 10 m/s of two diverging pencils are depicted in figure 3.6(b). The simulations are done for a diverging channel with an angle of $\theta = 2.5°$ and a channel with an angle of $\theta = 1.25°$. The figure shows velocity profiles which are not related to a Poiseuille profile, but it can bee seen that the velocity gradient is much lower than the velocity gradient

Table 3.7: Flow development of the brass, deck-plate burners

R [mm]	0.4	0.4	0.4	0.8	0.8	0.8
$\bar{v}$ [m/s]	10	25	50	10	25	50
V_{max} [m/s]	18.1	38.8	70.1	14.3	32.2	60.6
$V_{max,p}$ [m/s]	20	50	100	20	50	100
V_{max}/V [m/s]	1.81	1.55	1.40	1.43	1.29	1.21
α_p	0.68	0.38	0.25	0.27	0.17	0.12
g/g_p	1.12	1.41	1.75	1.68	2.22	2.85

Table 3.8: Flow development of the brass, converging channel, pencil burner

$\bar{v}$ [m/s]	10	50	100
V_{max} [m/s]	12.1	53.5	103.1
$V_{max,p}$ [m/s]	20	100	200
$V_{max}/\bar{v}$ [m/s]	1.12	1.07	1.03
α_p	0.064	0.036	0.015
g/g_p	5.02	7.70	17.4

of a straight and a converging channel at 10 m/s. The problem of the diverging pencil is the possibility of boundary layer detachment resulting in a back-flow at the rim, which arises already at $\theta = 2.5°$. In figure 3.6(b), only the 10 m/s profile is shown, because it was not possible to obtain a converged solution for both the channel angles. This is also not solved by positioning the pressure outlet far away from the outlet. But during these iterations, a back-flow was present for both angles. This might be a result of the fact that the flow cannot be considered being incompressible at velocities higher than 70m/s.

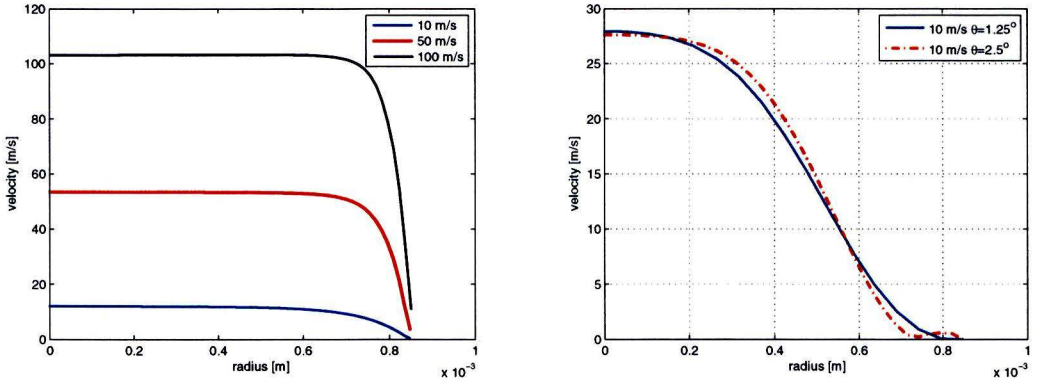

(a) Converging pencil burner

(b) Diverging pencil burners with angles of $\theta = 2.5°$ and $\theta = 1.25°$

Figure 3.6: Axial velocity flow profiles of the new designed pencil burners

3.2.3 2D flames

The two dimensional flames can be modeled in two manners, symmetrical and axisymmetrical. The symmetrical case can be considered to be a slit burner and the axisymmetrical case to be a cylindrical burner.

3.2.4 Boundary conditions

The boundary conditions for the two dimensional flame modeling described below are depicted in figure 3.7.

- (1) Symmetry boundary
  When modeled axisymmetrical, the symmetry is modeled as an axis. For a 2D flame a symmetry condition is modeled.

- (2) Outlet
  The outlet is modeled by means of a pressure outlet, this pressure is set to be atmospheric.
- (3) Outlet or burner wall
  Depending on the choice, this boundary is an outlet or a wall. When a free flame is modeled, this is a pressure outlet. When a flame in a box is modeled a burner wall is chosen.
- (4) Burner wall
  The burner wall is set to a constant temperature, and a non-slip condition is used.
- (5) Inlet
  The inlet will be given by a velocity profile, using the determined profiles from the figure 3.4.

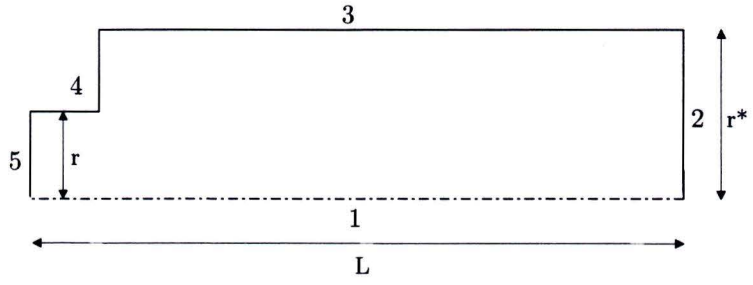

Figure 3.7: 2D flame

3.2.5 Burner flames

Lewis and von Elbe state that a wall temperature up to 100°C does not have a significant effect on flame stabilization [1, 6]. Observations at Philips Lighting BV, however, show that the blow-off velocities on the same burner setup are higher when the temperature of the burner is higher. Higher temperatures of the burner are observed when the burner is placed horizontal instead of vertical and when several burners are placed close together. For the simulations is chosen for a burner wall temperature of 300 K in all cases.
The flames are modeled steady state at first, because modeling time-dependently would require too much computational time. As stated in section 2.4, the implicit solver is used and at first, first order upwind schemes are used. The burner nozzle radius is in all cases r=0.85 mm, and r^*=2 mm as shown in figure 3.7. The length of the domain is L=5 mm, except when stated otherwise.

Free Flame

When modeling a free flame, boundary (3) in figure 3.7 is set as an pressure outlet.
Starting with a coarse grid of $2.5 \cdot 10^{-5}$ m, solving steady state with a first order upwind scheme, a mean inlet velocity of 7 m/s results in a flame traveling inside the tube. By raising the velocity to 15 m/s a laminar flame shape arises. The result can be seen in figure 3.8. In this figure the contours of the Arrhenius rate of reaction are shown, which is defined by equation (2.14). By plotting the rate of reaction, the contours and position of the flamefront can be visualized. The flamefront has some major abrupt transitions due to the coarse grid. Also it may be assumed

that, while using a coarse grid, the flame speed is overpredicted as shown by the pseudo 1D simulation in section 3.2.1. This results consequently in an underprediction of the flame height.

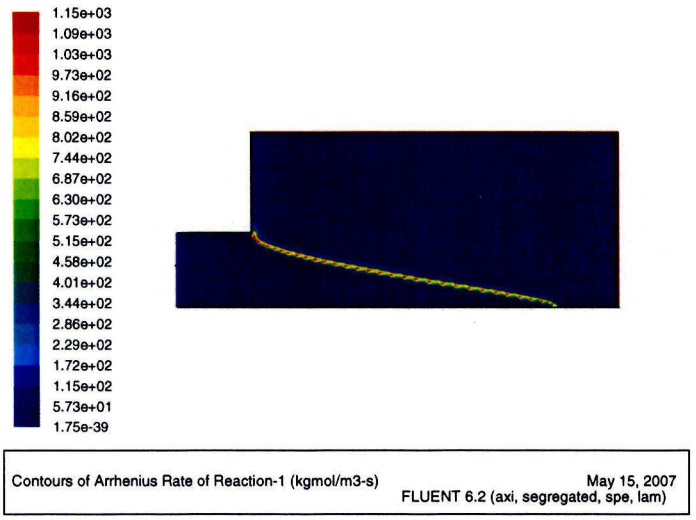

Figure 3.8: 2D axisymmetric free flame - grid size $2.5 \cdot 10^{-5}$ m - $\bar{v}$=15m/s

To check if a second order upwind scheme would predict a different result on this coarse grid, this is also modeled. This results in a raise in flame height. When figure 3.9 is compared with figure 3.8, one can see the drop in rate of reaction causing the flame to gain height.

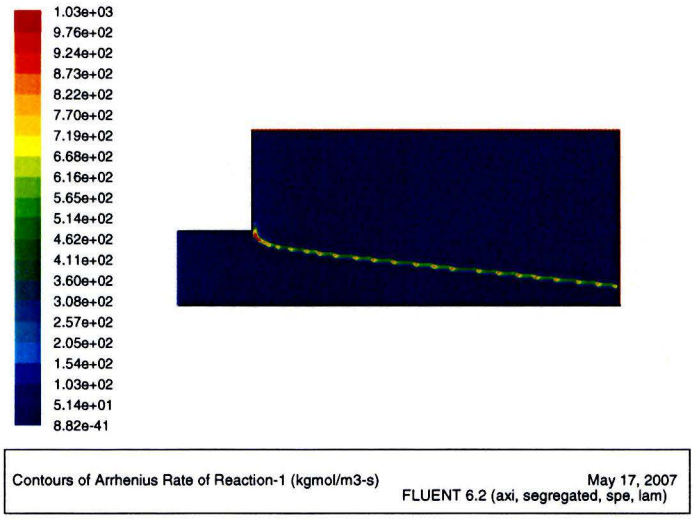

Figure 3.9: 2D axisymmetric free flame - grid size $2.5 \cdot 10^{-5}$ m - $\bar{v}$=15m/s -2nd order upwind

When refining the grid size, by a factor of two, the flame front is not straight anymore, but it wiggles and wrinkles. This is observed when the grid is refined three times to grid sizes of $3.125 \cdot 10^{-6}$ m as well.

In order to know if the wrinkling on small grid sizes is caused by using the segregated solver, the coupled solver is used on all grid sizes up to $3.125 \cdot 10^{-6}$ m. But in all cases the solution diverges within 1000 iterations.

Flame in a Box

To be sure that the instabilities described above are not influenced by the pressure outlet boundary, the flame will be modeled in a box. When modeling a flame in a box, boundary (3) in figure 3.7 is a wall. In this case the wall has the same properties as the burner wall and is set to 300 K with no-slip conditions. The solution on the coarse grid can be seen in figure 3.10, showing exactly the same result as the free flame on the same grid size in figure 3.8.

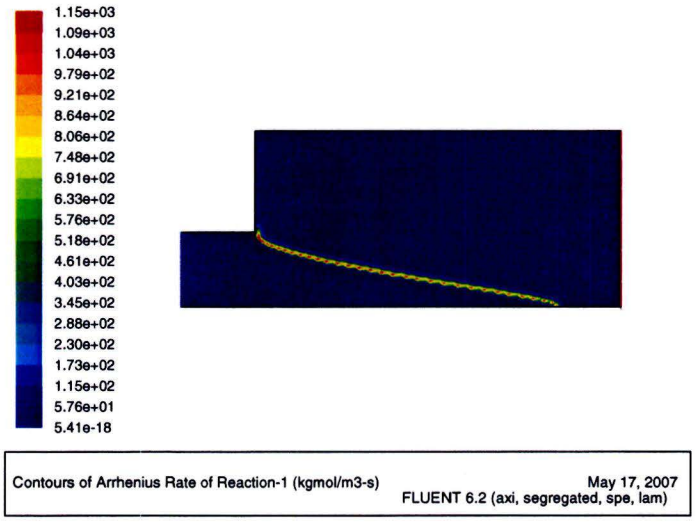

Figure 3.10: 2D axisymmetric flame in a box - grid size $2.5 \cdot 10^{-5}$ m - $\bar{v}$=15m/s

In this case, the same kind of wrinkling occurs as in the free flame case at smaller grid sizes. When the coupled solver is used in this configuration this leads also to divergence.

Impinging flame

While both the flame in a box and the free flame suffer from instabilities at smaller grid sizes than $2.5 \cdot 10^{-5}$ m, the flame is also modeled impinging to a wall. It is known that by putting an object, bluff body or flame holder in the burnt gasflow, results in a stabilization of the flame. The solution of the free flame is used as initial solution for the impinging flame. The outlet(2) is changed into a wall, with a chosen temperature of 1100K, chosen according to measurements from Remie [3]. The wall is positioned on a distance of L=5 mm, so the distance between the flame and the plate is only 2/3 millimeter. In figure 3.11 can be seen that the flame position does not change. The radial and axial velocity are shown in appendix E in figures E.1 and E.2, which correspond to the values as one would expected.

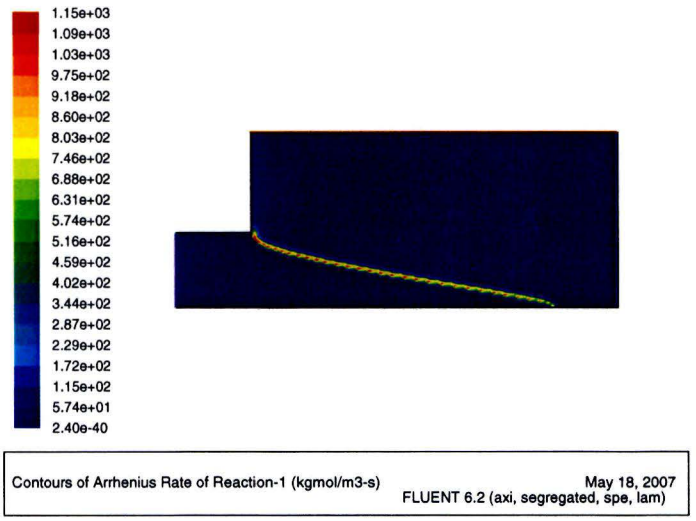

Figure 3.11: 2D axisymmetric impinging flame on a wall- grid size $2.5 \cdot 10^{-5}$ m - $\bar{v}$=15m/s - Reaction rate

Unsteady calculations

The simulations above are all performed using the steady state solver, but the wiggles on smaller grid sizes are still not explained, therefore unsteady calculations are performed.
On the coarse grid size $2.5 \cdot 10^{-5}$ m, time steps of $1 \cdot 10^{-6}$ seconds are allowed, when looking at table 3.5 of the pseudo 1D calculations. But to investigate the dependence on time-step also time steps of $1 \cdot 10^{-5}$ seconds are made. The result of the unsteady calculation on the coarse grid with time steps of $1 \cdot 10^{-6}$ seconds is shown in figure 3.12. In this figure one can see that the flamefront stays on the same position as for the steady cases. The predicted reaction rate however is higher as in the steady state cases. When time steps of $1 \cdot 10^{-5}$ seconds are made, the solution is given by figure 3.13. In this figure a even higher reaction rate is predicted, but in contradiction with theory, the flame height is higher compared to the simulation where smaller time-steps are made. This implies that when using times steps of $1 \cdot 10^{-5}$ seconds on a grid size of $2.5 \cdot 10^{-5}$ m, the time steps are too large to resolve the reaction.
The prediction of the flamefront on the refined grid is shown in figure 3.14. The flamefront on the refined grid shows the same kind of wiggles as for the unsteady cases, which do not disappear when calculating using a second order upwind scheme as is shown in figure 3.15.

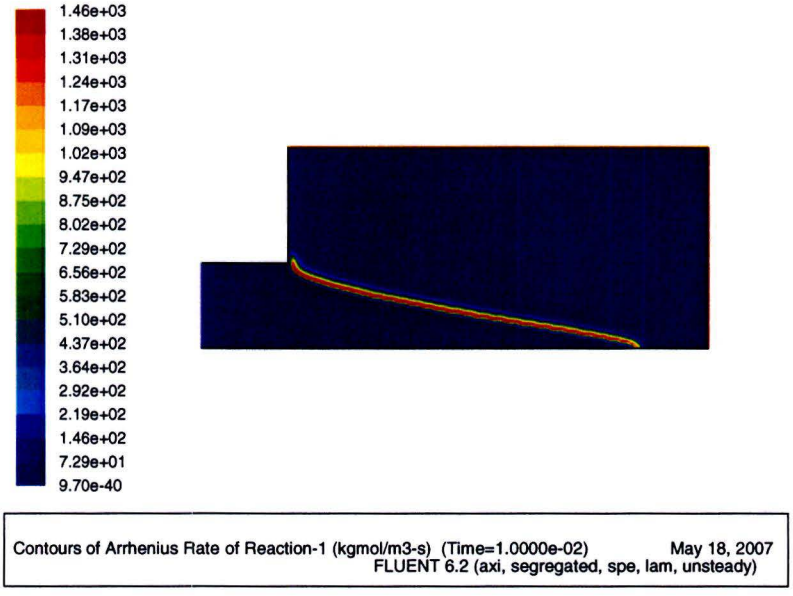

Figure 3.12: 2D axisymmetric free flame - unsteady - 1e-6 time steps - 1e-2sec -grid size $2.5 \cdot 10^{-5}$ m - $\bar{v}$=15m/s

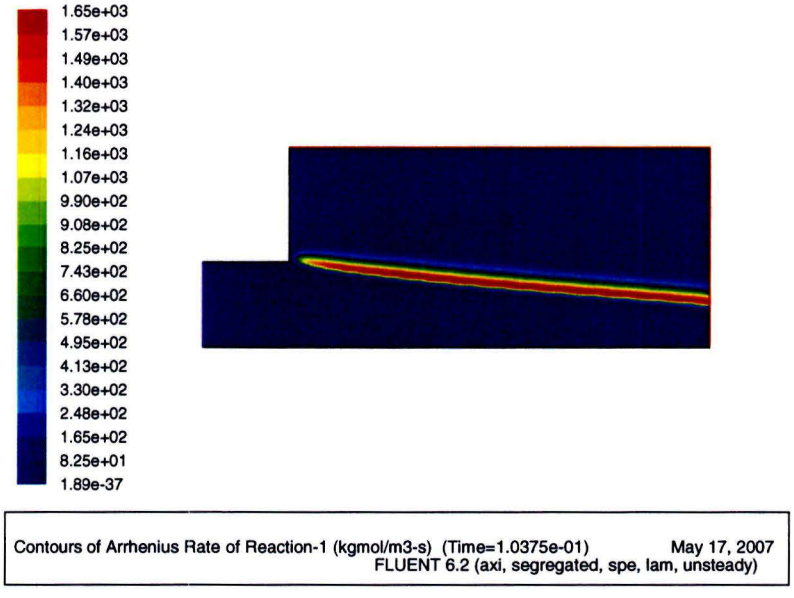

Figure 3.13: 2D axisymmetric free flame - unsteady - 1e-5 time steps - 0.1sec -grid size $2.5 \cdot 10^{-5}$ m - $\bar{v}$=15m/s

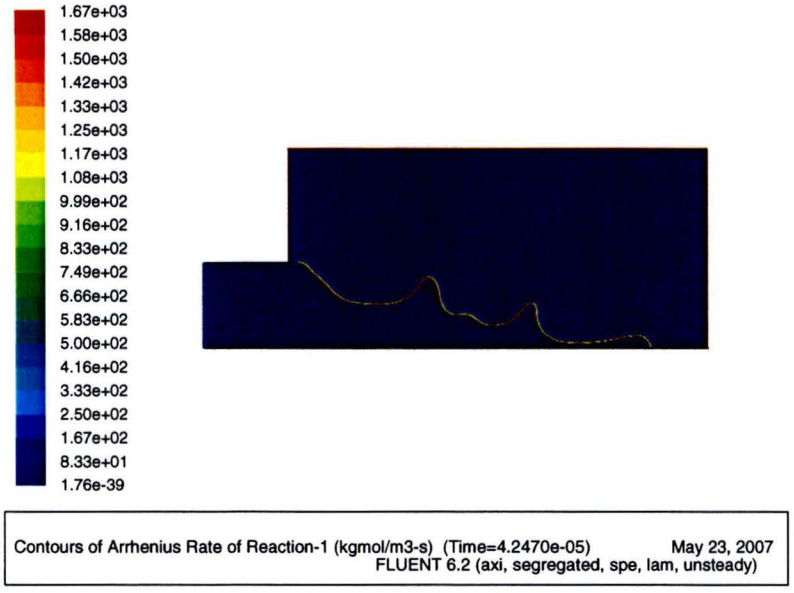

Figure 3.14: 2D axisymmetric free flame - unsteady - 1e-8 time steps - 4.25e-5sec - grid size $3.125 \cdot 10^{-6}$ m - $\bar{v}$=15m/s

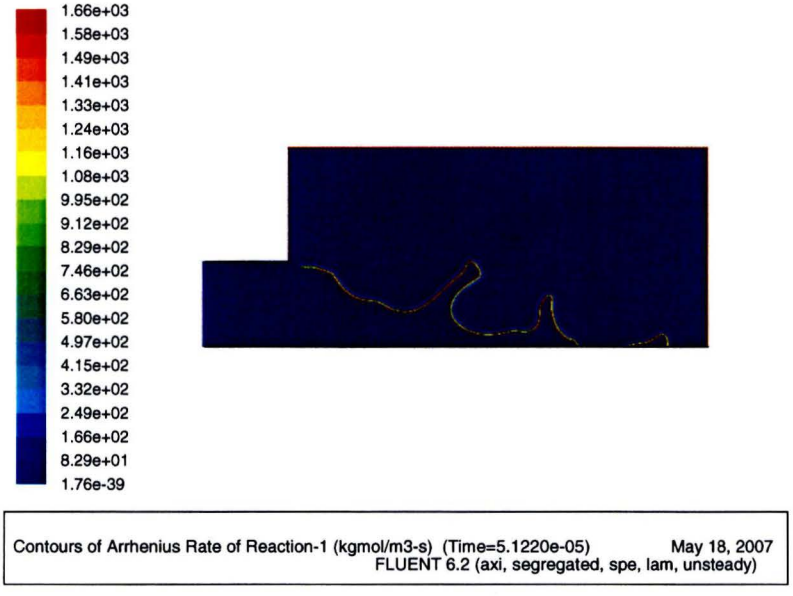

Figure 3.15: 2D axisymmetric free flame - unsteady - 2nd order - 1e-8 time steps - 5.12e-5sec - grid size $3.125 \cdot 10^{-6}$ m - $\bar{v}$=15m/s

3.3 Conclusions

It is possible to model the oxy-fuel flame with a one-step reaction which describes the flame properties well, except the flame thickness. Resulting in the need for a finer grid in the neighborhood of the flamefront than when modeling the flame using a larger reaction mechanism.
From the extensive pseudo-1D test case simulations of the methane-air flame it can be concluded that there is almost no difference in the results when modeling inlet diffusion, diffusion models and approximations for the specific heat. However it is very important to use the same conductivity approximation as used in the *Chem1D* calculations.
The pseudo-1D test case in *Fluent* produces the expected results. When refining the grid, the prediction of the flame speed is improved. But when computing time-dependently a finer grid needs smaller time steps, which results in large computing times, even for the pseudo 1D test-case. The regular pencil shape produces a far from developed Poiseuille flow profile at the outlet, and the converging geometry results in even higher boundary gradients. The pencil with a diverging channel geometry produces a flow profile with lower boundary velocity gradients, but the viscous boundary layer tends to detach from the wall at higher velocities then 10m/s, resulting in a slight back-flow.

When calculating steady state in the 2D simulation using the segregated solver and 1st order upwind, a coarse grid of $2.5 \cdot 10^{-5}$ m is able to predict the position of the flamefront fairly accurate. When solving it with the second order upwind scheme, the position of the flamefront changes, resulting in a higher flame. A higher order scheme suffers less from numerical diffusion than a first order approach, resulting in a better flame speed prediction, which is also shown in the pseudo-1D test case simulations in section 3.2.1.
When refining the grid size, up till $3.125 \cdot 10^{-6}$ m, the flame front is not straight anymore, but it shows wiggles which are not solved so far. Therefore it is until this moment not possible to determine the blow-off numerically. The flame in a box and the impinging flame on the coarse grid do not predict another position of the flamefront than the free flame.

Chapter 4

Experiments

In this chapter the blow-off gradient is determined experimentally by measuring the blow-off velocities. The goal of the experiments is to measure the blow-off velocities of different burner geometries to verify the derived equations derived for the blow-off gradient, which are described in section 1.2. At first the used burners will be described, together with more information of the development and production of new internal burner geometries. Secondly, the set-up and the performed experiments including the results are described into detail.

4.1 Burners

There are two types of burners used in this study: the "injector" burner (4.1(a)), where the fuel and oxidizer streams are premixed just before the outlet by using an injector and the "pot" burner in figures 4.1(c), where the fuel and oxidizer streams are mixed far before the outlet. The burner tubes which are positioned on the injector are called the "pencils", because of the

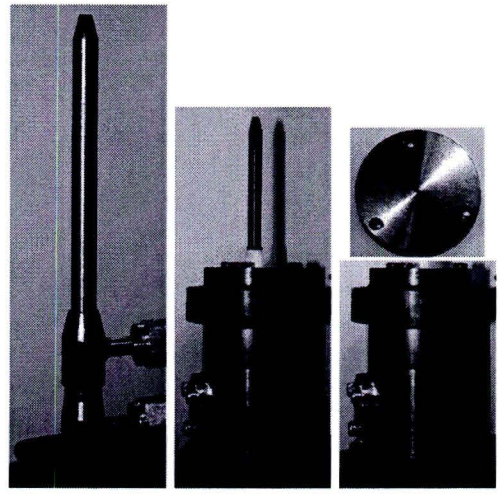

(a) (b) (c)

Figure 4.1: Burners

similarity with a real pencil. It is expected that the injector introduces turbulence and that the flame would behave different on this burner then when using the "pot" burner, which is assumed to be completely laminar. In this section the design, production and flow characterization of the pencil burner are described.

4.1.1 Design

To investigate if a different internal burner channel geometry of the pencil will influence the blow-off velocity, two new pencils are designed, both based on the industrial pencil with a straight channel used at Philips Lighting BV represented in figure 4.2(a). One pencil is equipped with a diverging channel at the end, figure 4.2(b) and another pencil with a converging channel 4.2(c). The outflow diameter of all pencils is kept equal to the original pencil, being 1.7 millimeters. The angle of the diverging pencil is designed to be $\theta = 2.5°$, and the restriction diameter is 1 mm at 8 mm from the outflow. The restriction of 1 mm has an area 3 times smaller than the diameter of 1.7 mm, raising the velocity 3 times, and thus raising Reynolds number with a factor of approximately 1.8 times. The increase in velocity sets limits to the assumption of the incompressibility of the gas. The Mach number (M) describing the ratio of the flow velocity (V) and the velocity of sound (c), $M = V/c$, is becoming too high. To assure incompressible flow, $M^2 << 1$, which holds with a speed of sound of $c = 340$ m/s for a flow velocity of about V=70 m/s [25]. This is also the explanation for not being able to obtain a converging solution of the determination of the flow profile of the diverging pencil in section 3.2.2.
To investigate if the production procedure has any influence on the blow-off velocities, the pencil with a straight "regular"channel shape is also produced, as will be described in the section below. By producing the straight regular channel pencil we are able to investigated the behavior of the regular geometry on the "pot" burner.

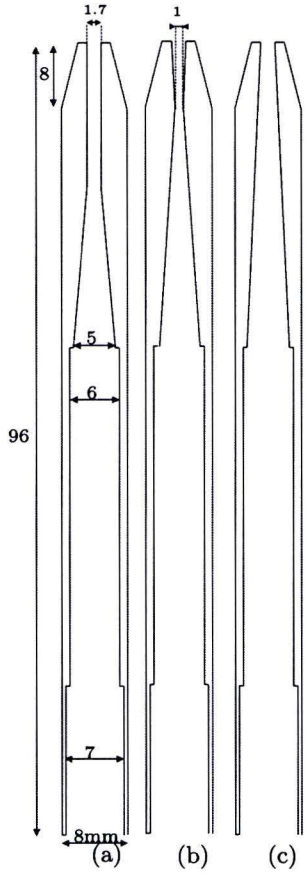

Figure 4.2: Pencil burners: Straight (a), Diverging (b), Converging (c), sizes are in mm

Production of the pencils

The channels are conical and formed using "zinc sparking". This zinc sparking is very difficult when using stainless steel because it is very hard. Therefore, brass is chosen to use as burner material. The use of brass is justified in this case because the burner does not heat up to the extent observed in industrial applications. The burner does not heat up because it is positioned vertically, without other burners or heat sources in the neighborhood. The newly designed pencil burners are provided with thread to be mounted on top of a pot burner, see figure 4.1(b), or placed on the injector of the pencil burner setup, like in figure 4.1(a).

Flow development

As described in section 1.2, the blow-off of flames depend on Reynolds number.
In table 4.1, the Reynolds numbers are given for a specific averaged velocity ($\bar{v}$) of 100 m/s. From this table can be concluded that the transition from laminar into turbulent at $Re = 2300$

happens at a mean velocity of about 22 m/s. The flow will be completely turbulent (Re=5000) at a velocity of about 47 m/s. After the flamefront the viscosity rises dramatically (due to high temperatures and a lower density), resulting in a fully laminar flow. The diameter of the flame after the flamefront is described by Remie, being $D_j = \sqrt{\tau} D_b = \sqrt{12.6} D_b = 3.55 D_b$, where τ is the expansion coefficient [3].

Table 4.1: Reynolds for CH4/O2 flow at ϕ=1.0

	Before flame 300K	After flame 3050K
D [m]	$1.7 \cdot 10^{-3}$	$6.0 \cdot 10^{-3}$
$\bar{v}$ [m/s]	100	100
ρ [kg/m^3]	1.08	$1.08 \cdot 10^{-1}$
μ [kg/(ms)]	$1.74 \cdot 10^{-5}$	$9.17 \cdot 10^{-5}$
ν [m^2/s]	$1.61 \cdot 10^{-5}$	$8.49 \cdot 10^{-4}$
Re [-]	10559	707

4.2 Set-up

In the burner set-up, mass-flow controllers (MFC's) are used to control the flow of fuel and oxygen. These MFC's are connected to a "multilab"providing the signal. The "multilab"is in turn connected to a computer with software to control the MFC's. The MFC's are mounted on a board and via valves can be chosen to premix the flows for the "pot" burner or to leave the flows separate for the pencil injector. The mass flow controllers all have a maximum flow, which in turn determines the maximum velocity that can be achieved in a specific burner. The averaged velocity through a burner hole, the surface of the hole and the ambient temperature are the input parameters. The program calculates the flow through the MFC's. The error in the control of the mass flow, when calibrated, is about 2%.

4.3 Blow-off measurements

Blow-off experiments are performed for two types of burners: the deck plate burner and the pencil shaped burner, and three types of burner set-ups: the deck plate on the "pot" burner, the brass pencils mounted on the "pot" burner and the pencils on the injector.

4.3.1 Deck-plate burner

The deck plate burners were also used by Van Zwieten [4] and Gerth [5] and show wear around the edges. This is observed with the naked eye. To investigate the effect of this curvature due to wear, two new deck plates with a radius of approximately 0.4 and 0.8 millimeters are made. All deck plates have a thickness of 1 cm.

The new deck plates do not have a curved outlet, the burner rim has an almost straight angle. To see how big the curve of the burner rim is exactly, microscopic pictures of the deck-burner plates are made after the burner experiments, which are depicted in appendix D. By using an optical microscope the diameter of the holes can be measured very precisely. By using a confocal microscope also the curvature can be investigated. The technique of the confocal microscope is roughly as follows. With confocal microscopy can be focused on different heights, to determine

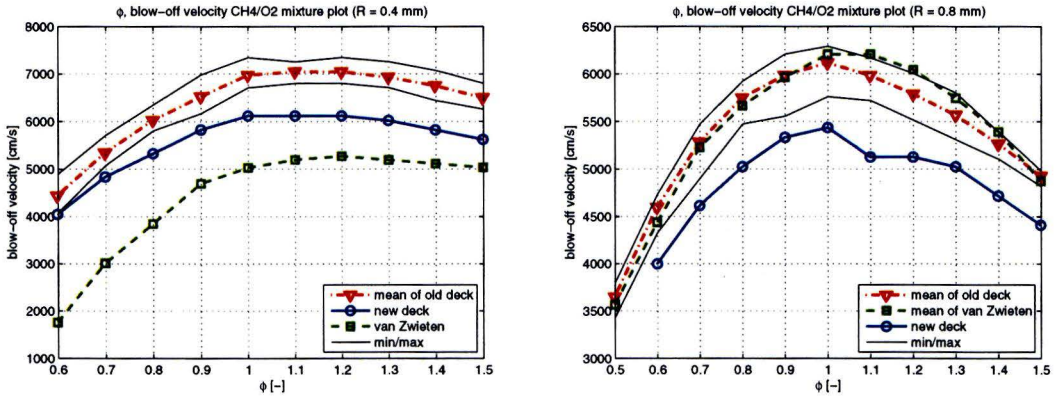

(a) R=0.4 mm (b) R=0.8 mm

Figure 4.3: Blow-off velocities of deck-plate burners

the specific height of the area which is in focus. The curvature of the new deck-plate burners is almost straight, even after using them to determine the blow-off velocities. But

The difference in diameter measured with the optical microscope, as can be seen in appendix D, is accounted for in the calculation of the velocity.

The measured blow-off velocities on the deck plates are shown in figure 4.3, where the ϕ on the x-axis stands for the stoichiometry. The mean velocities of the $R = 0.4$ mm burner are calculated out of 4 measurements and out of 5 measurements for the $R = 0.8$ mm burner.

The blow-off velocities measured by Van Zwieten [4] are plotted separate. The deviation between the measured blow-off velocities and those measured by Van Zwieten for the burner with a radius of $R = 0.4$ mm, can be prescribed to a change in set-up. But one would expect the same deviation between the measurements or the burner with a radius of $R = 0.8$ mm, and this is not the case. The min/max lines plotted in figure 4.3 are the minimum and maximum measured velocities. When neglecting the measurements by Van Zwieten, one be conclude from figure 4.3 that the blow-off velocity decreases when a straight outlet edge is used instead of a rounded one. This conclusion is valid because for these measurements the set-up is not changed.

During the experiments, it is observed that there is water condensation from the flame on the burner deck. Therefore it can be concluded that the burner deck does not heat up much. Heating up the burner rim to 50 degrees would prevent water from condensing [14], but this is not done during these measurements.

4.3.2 Pencil burners

The original steel pencil burner with straight outlet from Philips Lighting BV is only tested on the injector burner. The newly produced brass burners are also tested on the "pot" burner to investigate if the burner set-up influences the blow-off.

The blow-off results of the new brass pencil burners can be seen in figure 4.4(a), where the converging pencil on pot is a mean out of two measurements and the others are all single measurements. The blow-off velocities of the original steel Philips pencils, with straight channel, on the injector can be seen in figure 4.4(b), where the mean is calculated out of two measurements from two different burners.

When comparing figures 4.4(a) and 4.4(b), it can be concluded that the new-produced brass pencil with the straight internal profile performs less than a new original steel pencil from Philips. This can be ascribed to the production of the brass burners. Because the production process is very difficult and the holes should be produced by zinc sparking, there might be some difference in internal roughness which disturbs the velocity profile and thus resulting in a different blow-off velocity. The pencils are too long to be investigated by microscopy because no light from beneath the pencil will reach the detector in the microscope. Therefore the assumption that the internal geometry is the disturbing factor cannot be verified.

During the blow-off experiments it is observed that none of the pencil burners heats up when a high enough flow is applied. When the burner is lighted at a velocity of 30 m/s and the velocity is not raised, the burner will heat up.

Pictures of flames on the injector burner with the straight steel pencil, with different mean inlet velocity, can be seen in figure 4.5.

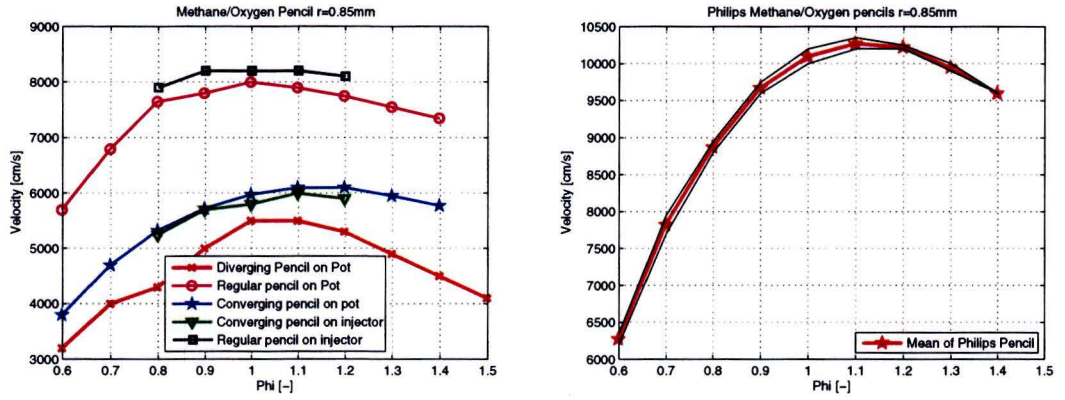

(a) New brass pencils

(b) New steel pencil with straight channel

Figure 4.4: Blow-off velocities of Pencil burners

4.4 Blow-off gradients

As described in section 1.2, the formulation for the blow-off gradient changes when the flow becomes turbulent. The blow-off velocities measured cause the flames to be in a regime where Reynolds is larger than 3000. This means that the blow-off gradient theory described by equation (1.9) should be used to determine the blow-off gradients. For the determination of the blow-off gradients it is chosen to compare the new deck plates, to be sure that the outflow geometries are the same.

When using the blow-off gradient theory presented by Reed, given by equation (1.4), and using s_l=3.05 m/s and the thermal diffusivity of the methane-oxygen mixture at 300K, $\alpha = 2.2 \cdot 10^{-5}$ the blow-off gradient would become $g_b = 9.7 \cdot 10^4$ 1/s. From this it can be concluded that the correlation from Reed is not applicable to methane-oxygen flames, while it differs too much from the blow-off gradient obtained by the experiments.

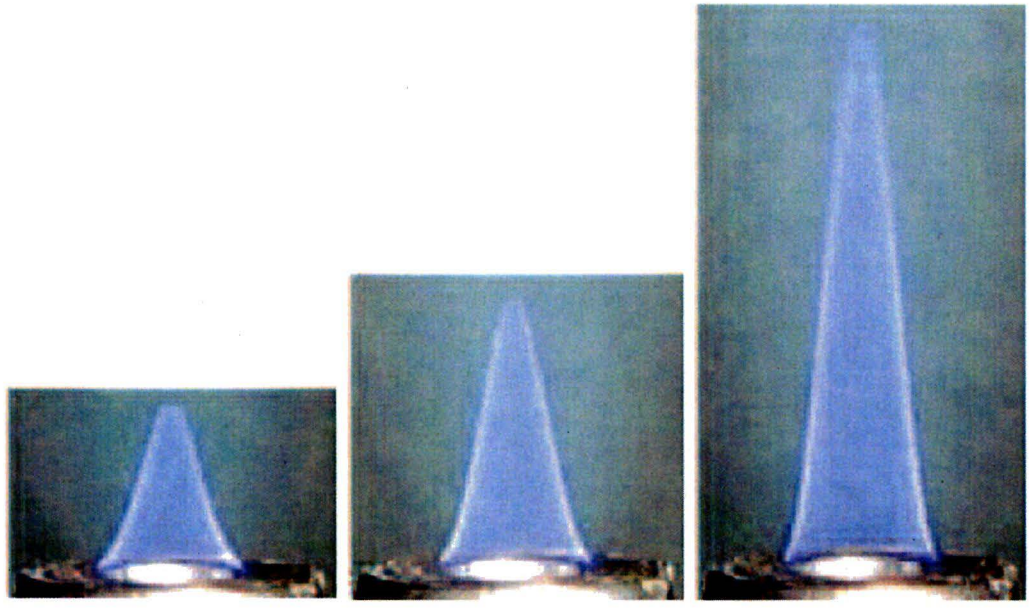

(a) 10 m/s: h≈2.3mm (b) 15 m/s (c) 30 m/s

Figure 4.5: Flames on a new steel Philips pencil a with straight channel, on the injector

4.4.1 Turbulent approach

As described above, the blow-off velocities are large enough to be in the turbulent regime, therefore equation (1.9) should be used to determine the blow-off gradients.

Table 4.2: Reynolds and boundary gradients for the new deck plates, straight steel and converging brass pencil burners at blow-off at ϕ=1.0, assuming turbulent flow, ν=1.61 $\cdot$ 10^{-5} m^2/s

Burner	deck plate	deck plate	straight steel pencil	converging brass pencil
D [m]	$0.8 \cdot 10^{-3}$	$1.6 \cdot 10^{-3}$	$1.7 \cdot 10^{-3}$	$1.7 \cdot 10^{-3}$
$\bar{v}$ [m/s]	70	62	100	60
Re [-]	3520	6161	10559	6335
g_b [1/s]	$12.5 \cdot 10^6$	$8.7 \cdot 10^6$	$20 \cdot 10^6$	$8.1 \cdot 10^6$

From table 4.2 it can be seen that the blow-off gradients of both new deck-plate burners differ about 30%. Following the theory, the blow-off gradient should not depend on the burner radius, so one would expect a larger blow off velocity of the R = 0.8 mm burner or a smaller blow-off velocity of the burner with a diameter of R = 0.4 mm. A large difference in blow-off gradient is also observed between the converging and straight channel pencil burner.
The reason for this deviation from the theory lies in the assumption that the flames are turbulent at a certain Reynolds number, but this assumption might not be applicable. There is not much time for the flow to become turbulent, because the channel length of the deck-plate burners, which is in both cases 10 mm and the length of the pencil channels of 17,5 mm are too short. In the converging channel pencil, the velocity raises by the decreasing area with a factor of

8.65 (from a diameter of 5 mm to 1.7 mm), which makes it even harder for the flow to become turbulent. From the large difference in the determined blow-off gradients using the turbulent theory can be concluded that for such short channel length the flow can probably not become turbulent. A rough estimation of the needed length to develop a turbulent boundary layer is given by: $Re = VL/\nu = 10^5$ [26].

Table 4.3: Approximation of the length needed for developing a turbulent boundary layer for the new deck plates, straight steel and converging brass pencil burners at blow-off velocity, ν=1.61 $\cdot$ 10^{-5} m^2/s

Burner	deck plate	deck plate	straight steel pencil	converging brass pencil
L_t [m]	$23 \cdot 10^{-3}$	$26 \cdot 10^{-3}$	$16 \cdot 10^{-3}$	$27 \cdot 10^{-3}$

In table 4.3 the approximated length needed for a boundary layer to become turbulent (L_t) at the blow-off velocities from table 4.2 are shown. From these values can be concluded that the straight steel pencil is the only burner where the Length of the channel (17.5 mm) is close to the length needed to developed a turbulent boundary layer. But as stated above, this is only an approximation, and the internal channel geometry does also influence the development of this boundary layer. The diameter changes gradually for the straight steel pencil from 5 mm to 1.7 mm as can be seen in figure 4.2(a), the estimation of $Re = 10^5$ might be to low. For the deck plates where the diameter changes from 40 mm to 0.4 of 0.8 mm, the estimation might be to high because an abrupt change might introduce a detachment already.

From the observations it is justified to conclude that the assumption of a turbulent flow can be rejected.

4.4.2 Laminar approach

When assuming that the channel length is to short to develop a turbulent flow, but also to short to develop a Poiseuille flow, one should define the boundary velocity gradient by equation (3.4), where $\alpha_p \neq 1$. The flow profiles used to determine the velocity gradient are depicted in figures 3.4 and 3.6(a).

For the measured blow-off velocity values of the new deck plate burners at ϕ=1.0, being approximately 61 m/s for the $R = 0.4$ mm hole and 54 m/s for the $R = 0.8$ mm hole, the blow-off gradient of the $R = 0.8$ mm hole differs almost 32% from the $R = 0.4$ mm hole. This can be seen in table 4.4. In this table also the blow off gradients are tabulated for the straight steel and converging brass pencil.

Table 4.4: Boundary gradients for the new deck plates at blow-off of the new deck plates at ϕ=1.0, assuming laminar flow

Burner	deck plate	deck plate	straight steel pencil	converging brass pencil
R [m]	$0.4 \cdot 10^{-3}$	$0.8 \cdot 10^{-3}$	$1.7 \cdot 10^{-3}$	$1.7 \cdot 10^{-3}$
$\bar{v}$ [m/s]	61	54	100	60
V_{max} [m/s]	80	64.7	121	63.6
α_p	0.20	0.11	0.12	0.031
g_b [1/s]	$1.2 \cdot 10^6$	$0.82 \cdot 10^6$	$1.34 \cdot 10^6$	$1.2 \cdot 10^6$

The blow-off gradients of the straight steel and the converging brass pencils and the $R = 0.4$ mm deck plate burner are in good agreement with each other. From this can be concluded that it is justified to assume a laminar flow for these channel lengths. The deviation of the $R = 0.8$ mm deck plate burner cannot be explained on this point, but a different roughness of the channel might be an explanation.

4.5 Pressure measurements

To know if the velocities measured in the laboratory can be reached at Philips lighting pressure measurements are performed. The pressures are only measured for an injector pencil burner, with a manometer (Euroindex S2520). The pressures are measured in the oxygen and methane ducts near the injector and the pencil with and without a burning flame and can be seen in figure 4.6. At Philips Lighting a gas supply network under a low constant pressure is available. The maximum speeds measured in the combustion laboratory can therefore never be reached in practice.
The hydrogen-oxygen flame clearly sounds like a turbulent flame above 200 m/s. The flame front, however, is still cone-shaped. The line of the oxygen pressure shows some drops, which are the result of reaching the maximum flow through the chosen mass-flow controllers and of the too large pressure drop over the whole set-up.
The pressure in the oxygen duct is much higher then in the methane and hydrogen duct, which means that the oxygen stream entrains the fuel from its duct, while the oxygen is fed into the injector from the lower duct in figure 4.1(a).

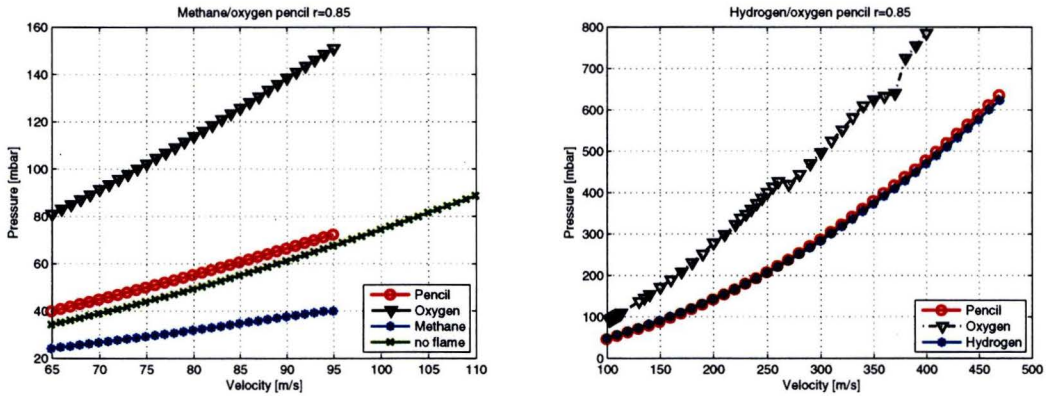

(a) Methane oxygen

(b) Hydrogen oxygen

Figure 4.6: Pressures in the pencil and in the fuel and oxidizer ducts

4.6 Conclusions

A curved outlet reaches higher blow-off velocities, which implies that the boundary velocity gradient has an influence on blow-off of the flames, and the assumption of determining the blow-off gradient using the velocity gradient is confirmed.
The Reynolds numbers imply a turbulent flow, but from the blow-off measurements of the deck plate burners it can be concluded that it is probably correct to assume that for the determination

of the blow-off gradient, the flow is still laminar. The blow-off velocities could, when applying the laminar blow-off theory, be much higher when the outflow profile would be fully developed before reaching the outlet. This is confirmed by the blow-off velocities of the burner hole with a radius of R=0.4 mm, which are in the same range as the blow-off velocities measured with the R=0.8 mm burner, while the flow profile is more developed in the R=0.4 mm deck plate burner, because the same channel length is used.
From the blow-off measurements of the pencil burners several conclusions can be drawn. First, there is almost no influence of the chosen burner type, "pot" or "injector" on the blow-off velocity. Second, the steel pencil provided by Philips Lighting BV reaches about 25% higher blow-off velocities than the brass pencils with the same geometry, which can be result of the producing precision. The blow-off velocities, and thus the blow-off gradient, of the diverging pencil are in correspondence with blow-off gradient result of the R=0.4 mm deck plate burner when the undeveloped laminar blow-off gradient theory is used.

Chapter 5

Discussion

The pseudo 1D test case in *Fluent* is able to predict the flame speed accurately comparing to the *Chem1D* calculations. However, the calculations show a great dependence on grid size and time step. When the grid size is refined, without reducing the time steps, the pressure will rise to non-physical heights, resulting in a divergent solution. To prevent this increase in pressure, time steps are reduced and taken in the order of $1 \cdot 10^{-9}$ s, at a grid size of $1.25 \cdot 10^{-6}$, which in turn results in large computational times.
The numerical results obtained by modeling a 2D axisymmetrical methane-oxygen flame of 15 m/s on a coarse grid size of $2.5 \cdot 10^{-5}$ m using the segregated solver and a 1^{st} order upwind scheme, are compared to a picture taken of the experimental burner set-up. Both are shown in figure 5.1. This figure shows that the flame height and the curvature are comparable. However, this comparison is questionable, due to fact that a coarse grid overpredicts the flame speed, and that the 2^{nd} order solution on the same grid size predicts a much higher flame.
When modeling a free axisymmetrical methane-oxygen flame, a transient behavior is observed when using small grid sizes. This could indicate that the flow is reacting on pressure oscillations introduced by the pressure outlet. This latter is not the case because the transient behavior is still present when the boundary condition is changed into a wall instead of a pressure outflow. The use of the coupled solver instead of the segregated, results in a divergent solution within 1000 iterations.
A possible explanation for this wiggling behavior of the flame can be found in the fact that the discretization is performed in the in x- and y- direction. The cone-shaped form of the flame results in high velocities perpendicular to the flame front, introducing numerical diffusion because the grid is not aligned with the flow direction. When a 2^{nd} order upwind scheme is used, which reduces the numerical diffusion, the solution still shows the same kind of wiggles.

When comparing the burner experiments, one can conclude that there is no essential difference between the blow-off velocities measured on "pot" and "injector" burners when the same pencil used. The expected influence of the injector on the blow-off by introducing turbulence is disproved by this experiment.
For the determination of the laminar blow-off gradients a correction is used for the fact that the flow-profiles are not completely developed into a Poiseuille profile ($\alpha_p \neq 1$). The results of the blow-off velocities obtained on the deck plate and the pencil burners can only be related to each other by using the laminar blow-off gradient theory, although Reynolds numbers are higher than 2000. This implies that the flow has no time to develop in a turbulent flame before reaching the end of the channel. This might be good, because a turbulent flame results in a better mixing of

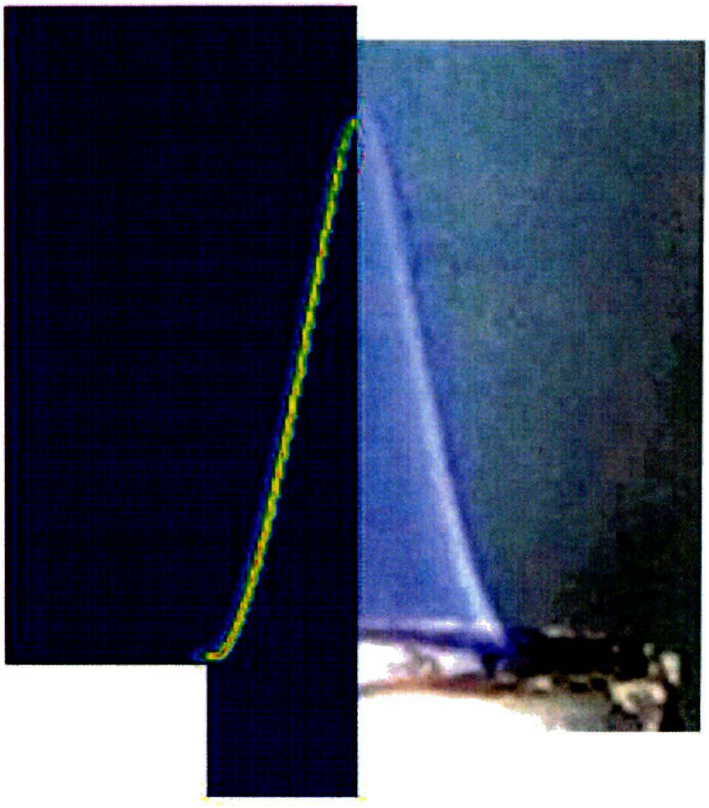

Figure 5.1: Comparison between the numerical and experimental of the flame stabilizing on a straight channel pencil burner with a mean velocity of 15 m/s

the burnt gases with the nitrogen in the ambient air, resulting in higher nitrogen oxides (NO_x) emission due to the high temperatures.
The design of the diverging pencil is not correct at high velocities. This is because the surface restriction in the pencil raises the velocity in such an extent that the flow cannot be considered incompressible anymore. Furthermore, the angle of $\theta = 2.5°$ of the diverging channel is too large, resulting in an unstable flame which wants to flash back near the rim.
Another observation concerning the deck plate flames is that when the flame is ignited by means of a spark from a lighter instead of a flame, the spark causes the flame to flash back into the pot burner at velocities where no flashback could be possible. This indicates that the spark is able to travel into the burner hole, causing a flashback.

Chapter 6

Conclusion

In the introduction of this thesis two objectives are stated:

- *Does the burner shape influence the blow-off velocity and is it possible to define the burner outlet in such a way that the flame attaches longer to the burner, to maximize the blow-off velocities of several burners?*
- *Is it possible to numerically determine the blow-off velocities using Computational Fluid Dynamics (CFD)?*

The burner shape influences the blow-off velocity, but not in very large amounts. However, the internal channel geometry is of essential importance for the performance of the burner. When the channel length is too short to develop a Poiseuille profile, the boundary gradient is much higher than for a developed flow, resulting in a lower blow-off velocity. It is, in principle, possible to design a pencil with a lower velocity gradient at the rim of the burner. Either by applying a larger channel length, or by designing a diverging channel geometry. For a methane-oxygen flame, the blow-off velocities are higher then for a methane-air flame, resulting in a compressible flow at the restriction of the diverging channel.

To numerically determine the blow-off velocities, an one-step mechanism is developed which has flame properties similar to the larger mechanisms *GRImech* and *Smooke*. This is proved by modeling the one-step mechanism in *Chem1D* and by using a pseudo-1D model in the Computational Fluid Dynamics package *Fluent*. With the current CFD model it is not possible to determine the blow-off velocities, because modeling the flame using the one-step mechanism on a fine grid size results in a transient behavior of the flamefront. The cause of this transient behavior is still unknown. However a flame similar to an experimentally observed flame shape is obtained using a coarse grid.

Besides the above results it is concluded that although Reynolds number is higher than 2000 at the measured blow-off velocities, the laminar blow-off theory can be applied for the determination of the blow-off gradients. This implies that the flow has no time to become turbulent in the short channel and may be considered as laminar. When developing a burner with a longer channel to obtain a developed Poiseuille profile, it might result in a fully turbulent flow because the turbulence has more length to develop.

Chapter 7

Recommendations

With the same straight channel geometry, the blow-off velocities of the new brass burner are lower than the blow-off velocities of the steel Philips burner. In this thesis it is stated that this difference might be due to differences in roughness of the channels. To confirm this statement it is recommended to investigate the exact surface and hole diameters by using optical and confocal microscopy as used in this study to investigate the deck-plate burners. This is not done because the burners have to be cut in pieces to apply these microscopic techniques.
As is shown in this thesis, the flow profiles at the outlet of the burners are not fully developed. It is recommended to design a burner with the same geometry but with an extended channel length to obtain a fully developed flow, to be able to check if the blow-off velocity can be raised. However a longer channel length might result in a transition into a turbulent flow. It is the challenge to find a optimum in the trade-off between a more developed profile and a transition into a turbulent flow. It is recommended to use *Fluent* to find an optimal channel geometry to decrease the boundary velocity gradient..
When the methane-oxygen flame can be modeled accurately using the computational fluid dynamics package *Fluent*, the model can also be extended. It is then, for instance, possible to investigate the interaction of flames by modeling several flames next to each other. It might also be possible to model an impinging flame including the heat transfer to the glass. However the exothermic recombination of dissociated species into stable species, the thermo-chemical heat release, cannot be taken into account because the dissociated species are not implemented in the developed one-step mechanism.

Chapter 8

Acknowledgement

I would like to thank the following people who have helped me during this study on the stabilization of oxy-fuel flames. Koen Schreel, Martin Remie and Philip de Goey for supervising me the past year. Jeroen van Oijen, Roy Hermanns and Rob Bastiaans for providing me with knowledge of *Chem1D* and *Fluent*. Bart Somers for helping adjusting some lines in *Chem1D*. Richard Mikkers for providing me with three brand new pencils and the detailed blueprint of the pencil burner. Cis Goris for the interesting tour at Philips Lighting Turnhout. Henri Vliegen, Geert-Jan van Hoek, Gerard van Hout and Gerard van Hattum for the technical help. Jan Hasker for helping with the IT related problems. Harry de Laat at the GTD for producing the brass pencils. Marc van Maris for helping me performing the microscopic pictures of the deck plate burners. And last but not least Tessa for the moral support and for reading this report.

Bibliography

[1] Lewis B. and von Elbe G. *Combustion, Flames and explosions of Gases.* Academic Press INC, New York, 2nd edition, 1961.

[2] Cremers M.F.G. *Heat Transfer of Oxy-Fuel flames to glass - The role of Chemistry and Radiation.* Ph.D. Thesis, Eindhoven University of Technology, 2006.

[3] Remie M. *Heat transfer by Oxy-fuel.* Ph.D. Thesis Eindhoven University of Technology, 2006. URL `http://www.combustion.tue.nl`.

[4] Zwieten F. van. *Blow-off of oxy fuel flames and air-fuel flames.* Bsc. final project, Eindhoven University of Technology, Rep. nr. WVT 2005.16, 2005. URL `http://www.combustion.tue.nl`.

[5] Gerth M.G. *Flame stabilization for Oxy-fuel flames.* Msc. thesis, Eindhoven University of Technology, Rep. nr. WVT 2004.13, 2004. URL `http://www.combustion.tue.nl`.

[6] Lewis B. and von Elbe G. Stability and structure of burner flames. *Journal of Chemical Physics*, 11:75–97, 1943.

[7] Harris M.E., Grumer J., von Elbe G., and Lewis B. Bunring velocities, quenching, and satbility data on nonturbulent flames of methane and propane with oxygen and nitrogen. *3rd symposium on combustion, flmae and explosion pheonmena*, 3:80–88, 1948.

[8] Reed Stuard B. Flame stretch - a connecting principle for blow-off data. *Combustion & flame*, 11:177–189, 1967.

[9] CHEM1D. 2007. URL `http://w3.wtb.tue.nl/nl/organisatie/combustion_technology/flamecodes/chem1d/`.

[10] Lange R. de. *Modelling of premixed laminar flames.* Ph.D. Thesis Eindhoven University of Technology, 1992.

[11] Smith G.P., Golden D.M., Frenklach M., Moriarty N.W., Eiteneer B., Goldenberg M., Bowman C.T., Hanson R.K., Song S., Gardiner W.C. Jr., Lissianski V.V., and Qin Z. URL `http://www.me.berkeley.edu/gri_mech/`.

[12] Smooke M.D. and Giovangigli V. Formulation of the premixed and nonpremixed test problems - reduced kinetic mechanisms for asymptotic approximations for methane-air flames - lecture notes in physics 384. 11:1–28, 1991.

[13] Bongers H. *Analysis of Flamelet-Based Methods to Reduce Chemical Kinetics in Flame Computations.* Ph.D. Thesis Eindhoven University of Technology, 2005. URL `http://www.combustion.tue.nl`.

[14] Mallens R.M.M. *Stabilisation of Laminar Premixed Methane/Air Flames.* Ph.D. Thesis Eindhoven University of Technology, 1996.

[15] Maaren A. van. *Onestep chemical reaction parameters for premixed laminar flames.* Ph.D. Thesis Eindhoven University of Technology, 1994.

[16] Somers L.M.T. *The simulation of flat flames with detailed and reduced chemical models.* Ph.D. Thesis Eindhoven University of Technology, 1994,.

[17] McGee H.A. *Molecular Engineering.* McGraw-Hill, New York, 1991.

[18] Kuo K.K. *Principles of combustion.* John Wily & sons, Inc. , New Jersey, 2005. ISBN 0-471-04689-2.

[19] Hirschfelder J.O., Curtiss C.F., and Bird R.B. *Molecular Theory of Gases and Liquids.* John Wiley & Sons, New York, 1954.

[20] Williams F.A. *Combustion Theory.* Addison-Wesley Publishing Company, Redwood City, 1985.

[21] Bongers H. and Goey L.P.H. The effect of simplified transport modeling on the burning velocity of laminar premixed flames. *Combustion science and technology*, 17:1915–1928, 2003.

[22] Fluent Inc. *Fluent manual - Using the solver.* 2005. URL `http://www.fluent.com`.

[23] Oijen J.A. *Flamelet-Generated Manifolds: Development and Application to Premixed Laminar Flames.* Ph.D. Thesis Eindhoven University of Technology, 2002. URL `http://www.combustion.tue.nl`.

[24] Warnatz J., Maas U., and Dibble R.W. *Combustion - Physical and chemical fundamentals, modeling and simulation, experiments, pollutant formation.* Springer Verlag Berlin Heidelberg, 1996.

[25] Schram P.P.J.M., van Heijst G.J.F., and van Dongen M.E.H. *Fysische transportverschijnselen voor werktuigbouwkunde, collegediktaat.* Eindhoven University of Technology, 1994.

[26] Lange R. de. *Personal conversation.* 2007.

Nomenclature

a	strain rate	[1/s]
A	area	[m^2]
A_r	pre-exponential factor	[consistent units]
c_p	specific heat at constant pressure	[J/kgK]
B	constant in the c_p-relation equations	[]
C	molar concentration	[m]
d	distance	[m]
D	diameter	[m]
$D_{i,m}$	mass diffusion coefficient for species i in mixture m	[m^2/s]
$D_{T,i}$	thermal diffusion coefficient	[m^2/s]
$\mathcal{D}_{i,j}$	binary mass diffusion coefficient of species i in species j	[]
E_r	activation energy	[J/mol]
f	friction coefficient	[-]
$\vec{F}$	external body forces	[N]
$\vec{g}$	gravitational acceleration vector	[m/s^2]
g_b	blow-off gradient	[1/s]
g_f	flashback gradient	[1/s]
h	distance between burner and glass	[m]
h	enthalpy	[J]
h_i^0	formation enthalpy of species i	[J]
H	height of domain	[m]
I	unit tensor	[-]
$\vec{J}_i$	diffusion flux	[kg/m^2s]
k	rate constant	[-]
k_B	Bolzmann constant $1.3807 \cdot 10^{-23}$	[J/K]
L	length of domain	[m]
$M_{w,i}$	molecular mass of species i	[m]
n	constant exponent in the c_p-relation equations	[-]
p	pressure	[Pa]
Q	flow	[m^3/s]
r	cylindrical coordinate	[m]
R	radius	[m]
R	universal gas constant (8.314)	[J/molK]
R_i	net rate of production of species i by chemical reaction	[kg/m^3s]
$\hat{R}_{i,r}$	Arrhenius molar rate of reaction if species i in reaction r	[mol/m^3s]
Re	Reynolds number	[-]
s_l	burning velocity	[m/s]
S_h	Source of energy due to chemical reaction	[]

t	time	[s]
T	temperature	[K]
T_A	activation temperature	[K]
T_f	flame temperature	[K]
$\vec{v}$	velocity vector	[m/s]
$\bar{v}$	averaged velocity	[m/s]
v_{in}	inlet velocity	[m/s]
$\vec{V}_i$	diffusion velocity	[m/s]
x	cartesian coordinate	[m]
X_i	mol fraction of species i	[m]
y	cartesian coordinate	[m]
Y_i	mass fraction of species i	[-]
z	cartesian coordinate	[m]

Greek letters

α	thermal diffusivity	[m^2 s]
α_p	flow development compared to fully developed Poiseuille flow	[-]
β	temperature exponent	[-]
δ	boundary layer thickness	[m]
δ_f	flame thickness	[m]
ϵ	depth of the potential well	[J]
η	rate exponent	[-]
θ	angle	[°]
λ	thermal conductivity	[W/mK]
μ	dynamic viscosity =molecular viscosity	[kg/ms]
ν	kinematic viscosity	[m^2/s]
$\nu_{i,r}$	stoichiometric coefficient for species i in reaction r	[m^2/s]
ρ	density	[kg/m^3]
Ω_D	diffusion collision integral	[]
σ_i	L-J characteristic length	[Å]
τ	expansion coefficient	[-]
$\bar{\bar{\tau}}$	viscous stress tensor	[-]

List of Figures

Appendix A

One-step properties

Methane-oxygen: Polynomials for the thermal diffusivity α, the viscosity μ and the conductivity λ, for a Lewis=1 flame with a c_p=3635 J/kgK. The polynomials of the viscosity and the conductivity describe the same dependence on the temperature as the c_p-relations, given in section 2.5.2 with the constants given in table 3.1.

$$\alpha = -6.86 \cdot 10^{-7} + 4.23 \cdot 10^{-9} \cdot \mathrm{T} + 7.95 \cdot 10^{-11} \cdot \mathrm{T}^2 - 6.75 \cdot 10^{-16} \cdot \mathrm{T}^3 \quad \text{(A.1)}$$

$$\mu = 5.57 \cdot 10^{-6} + 4.28 \cdot 10^{-8} \cdot \mathrm{T} - 7.42 \cdot 10^{-12} \cdot \mathrm{T}^2 + 9.13 \cdot 10^{-16} \cdot \mathrm{T}^3 \quad \text{(A.2)}$$

$$\lambda = 1.4 \cdot 10^{-3} + 9.86 \cdot 10^{-05} \cdot \mathrm{T} - 2.91 \cdot 10^{-9} \cdot \mathrm{T}^2 + 3.23 \cdot 10^{-3} \cdot \mathrm{T}^3 \quad \text{(A.3)}$$

Methane-air: Polynomials:

$$\mathrm{c_p} = 910.85 + 5.65 \cdot 10^{-01} \cdot \mathrm{T} - 1.53 \cdot 10^{-04} \cdot \mathrm{T}^2 + 9.82 \cdot 10^{-09} \cdot \mathrm{T}^3 \quad \text{(A.4)}$$

$$\lambda = 4.72 \cdot 10^{-03} + 7.60 \cdot 10^{-05} \cdot \mathrm{T} + 3.63 \cdot 10^{-10} \cdot \mathrm{T}^2 - 1.70 \cdot 10^{-12} \cdot \mathrm{T}^3 \quad \text{(A.5)}$$

$$\alpha = -1.50 \cdot 10^{-5} + 8.45 \cdot 10^{-8} \cdot \mathrm{T} + 1.14 \cdot 10^{-10} \cdot \mathrm{T}^2 - 4.91 \cdot 10^{-15} \cdot \mathrm{T}^3 \quad \text{(A.6)}$$

Lewis numbers for a methane-air flame, as first derived by Smooke [12]:

CH_4	0.97
O_2	1.11
N_2	1.00
H_2O	0.83
CO_2	1.39

Appendix B

Axisymmetric conservation equations

$$\frac{\partial \rho}{\partial t} + \frac{\partial \rho}{\partial x}(\rho v_x) + \frac{\partial \rho}{\partial r}(\rho v_r) + \frac{\rho v_r}{r} = 0 \tag{B.1}$$

The conservation of momentum:

$$\frac{\partial}{\partial t}(\rho v_x) + \frac{1}{r}\frac{\partial}{\partial x}(r\rho v_x v_x + \frac{1}{r}\frac{\partial}{\partial r}(r\rho v_r v_x) = -\frac{\partial p}{\partial x} + \frac{1}{r}\frac{\partial}{\partial x}\left[r\mu\left(2\frac{\partial v_x}{\partial x} - \frac{2}{3}(\nabla \cdot \vec{v})\right)\right] \frac{1}{r}\frac{\partial}{\partial r}\left[r\mu\left(\frac{\partial v_x}{\partial r} + \frac{\partial v_r}{\partial x})\right)\right] + F_x \tag{B.2}$$

The energy equation:

$$\frac{\partial}{\partial t}(\rho E) + \nabla \cdot (\vec{v}(\rho E + P)) = \nabla \cdot \left(k_{\text{eff}} \nabla T - \sum_j h_j \vec{J}_j + (\bar{\bar{\tau}}_{\text{eff}} \cdot \vec{v})\right) + S_h \tag{B.3}$$

$$\frac{\partial}{\partial t}(\rho Y_i) + \nabla \cdot (\rho \vec{v} Y_i)) = -\nabla \cdot \vec{J}_i + R_i + S_i \tag{B.4}$$

Appendix C

Derivation of the blow-off gradient for a non developed Poiseuille profile

For a non developed Poiseuille profile holds:

$$v(r) = V_{max}\frac{R^2 - r^2}{R^2} = V_{max}\left(1 - \left(\frac{r}{R}\right)^{\frac{1+\alpha_p}{\alpha_p}}\right) \tag{C.1}$$

In which α_p represents the factor of being a fully developed Poiseuille profile, when α_p=1, the flow is fully developed.

$$\begin{aligned}
\pi R^2\bar{v} = 2\pi\int_0^R v(r)rdr &= 2\pi V_{max}\int_0^R\left(1 - \left(\frac{r}{R}\right)^{\frac{1+\alpha_p}{\alpha_p}}\right)rdr \\
&= 2\pi V_{max}\int_0^R\left(r - \frac{r^{(\frac{1+\alpha_p}{\alpha_p}+1)}}{R^{\frac{1+\alpha_p}{\alpha_p}}}\right)dr \\
&= 2\pi V_{max}\left[\frac{1}{2}r^2 - \left(\frac{1}{R^{\frac{1+\alpha_p}{\alpha_p}}}\cdot\frac{1}{\frac{1+\alpha_p}{\alpha_p}+2}\cdot r^{(\frac{1+\alpha_p}{\alpha_p}+2)}\right)\right]_0^R \\
&= 2\pi V_{max}\left(\frac{1}{2}R^2 - \left(\frac{1}{\frac{1+\alpha_p}{\alpha_p}+2}R^2\right)\right) \\
&= 2\pi V_{max}R^2\left(\frac{1}{2} - \frac{1}{\frac{1+\alpha_p}{\alpha_p}+2}\right)
\end{aligned} \tag{C.2}$$

From equation C.2 the equation for the mean velocity can be derived.

$$\bar{v} = V_{max}\left(\frac{1}{2} - \frac{1}{\frac{1+\alpha_p}{\alpha_p}+2}\right) = V_{max}\frac{1+\alpha_p}{1+3\alpha_p} \tag{C.3}$$

The derivation of the blow-off gradient is as follows:

$$g_b = \lim_{r \to R} \left(- \frac{dv}{dr} \right) = \lim_{r \to R} \left(- \frac{d\left(\left(1 - \frac{r^{\frac{1+\alpha_p}{\alpha_p}}}{R^{\frac{1+\alpha_p}{\alpha_p}}} \right) V_{max} \right)}{dr} \right) = \frac{1+\alpha_p}{\alpha_p} \frac{1}{R} V_{max} \tag{C.4}$$

Appendix D

Microscopic pictures of the deck plates

For the determination of the wear and precise diameters of the outlet holes of the burners, pictures of the are made using optical microscopy. Confocal microscopy is used to look to the curvature of the burner rim into detail.

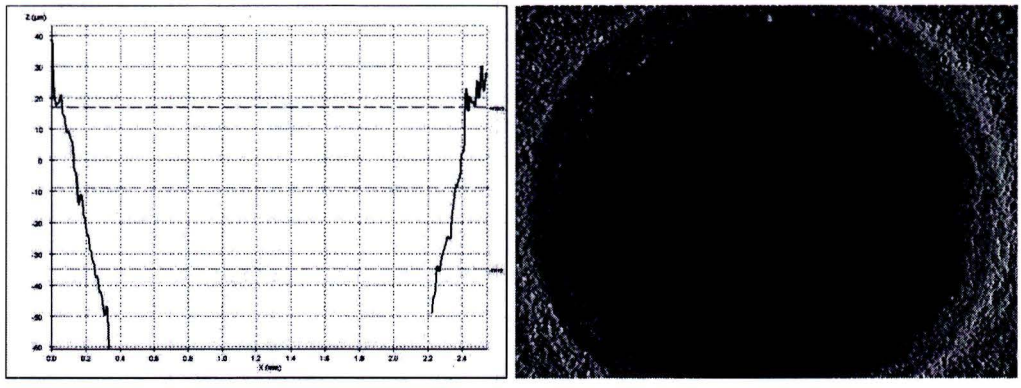

(a) Profile of the old burner

(b) Contour of the old burner

Figure D.1: Pictures of r≈0.8 mm burner holes using confocal microscopy

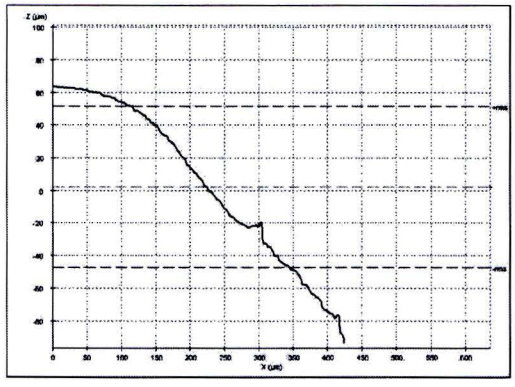

(a) Profile of the old burner

(b) Contour of the old burner

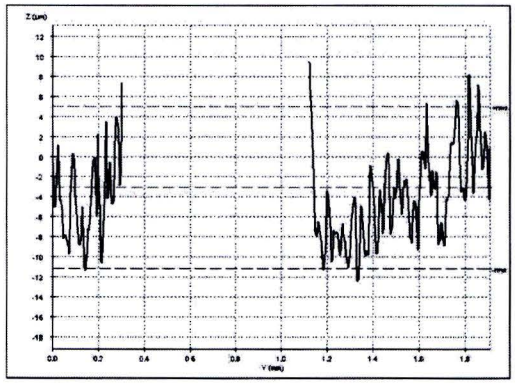

(c) Profile of the new burner

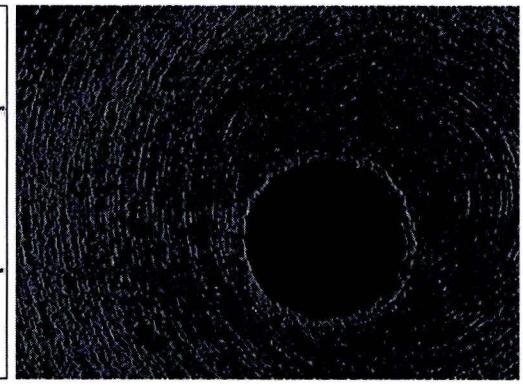

(d) Contour of the new burner

Figure D.2: Pictures of r≈0.4 mm burner holes using confocal microscopy

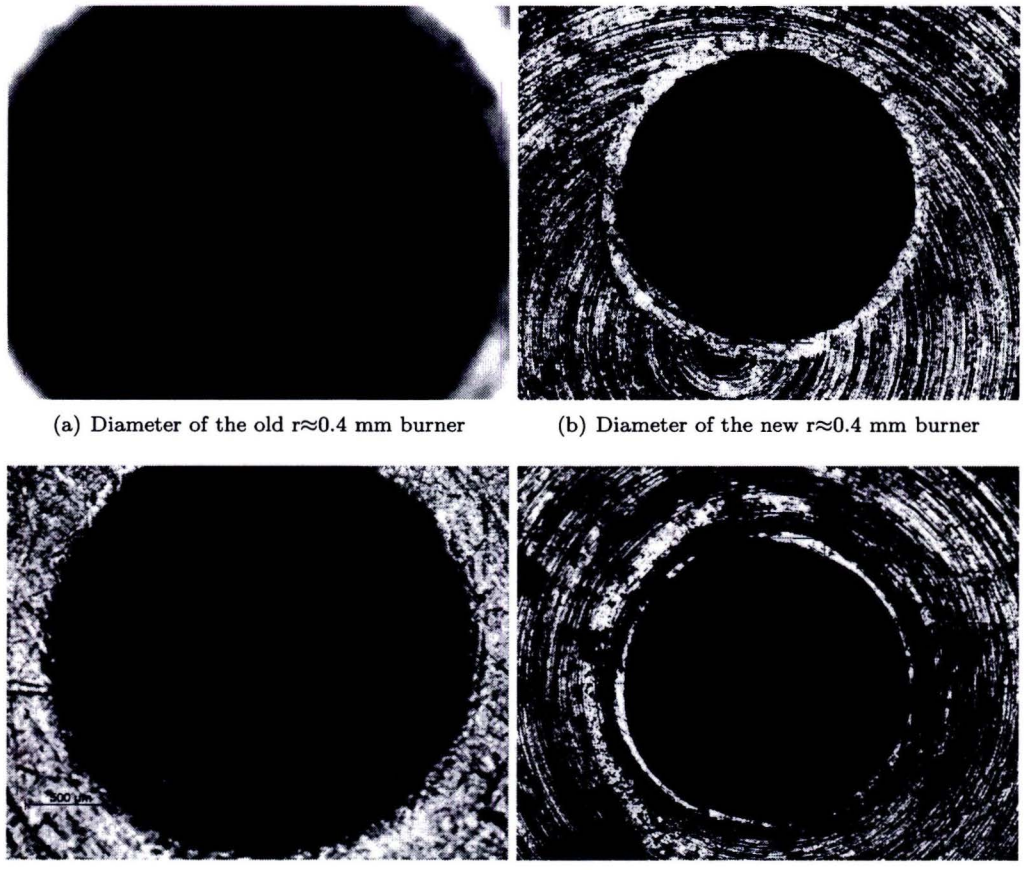

(a) Diameter of the old r≈0.4 mm burner

(b) Diameter of the new r≈0.4 mm burner

(c) Diameter of the old r≈0.8 mm burner

(d) Diameter of the new r≈0.8 mm burner

Figure D.3: Pictures of burner holes using optical microscopy

Appendix E

Velocity profiles of an impinging flame

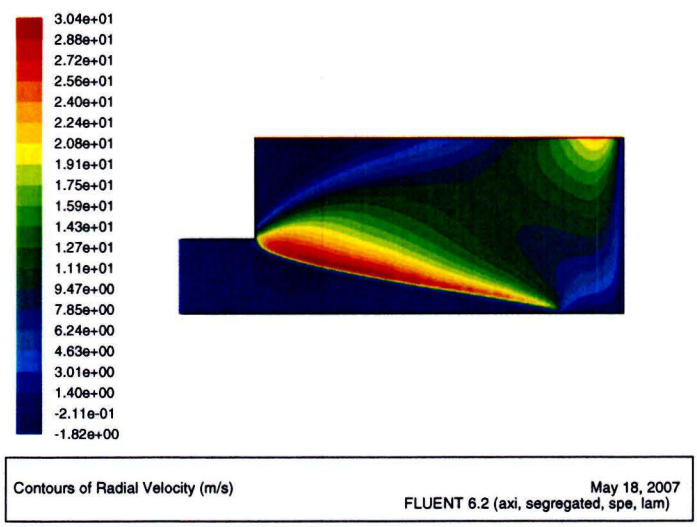

Figure E.1: 2D axisymmetric impinging flame on a wall- grid size $2.5 \cdot 10^{-5}$ m - $\bar{v}$=15m/s - radial velocity

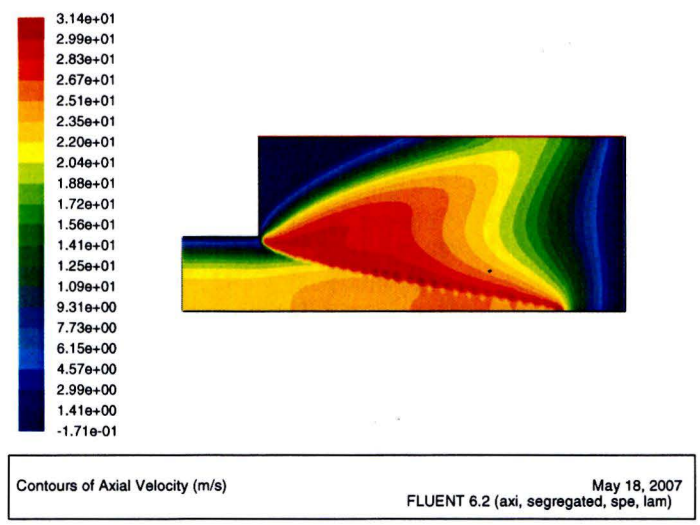

Figure E.2: 2D axisymmetric impinging flame on a wall- grid size $2.5 \cdot 10^{-5}$ m - $\bar{v}$=15m/s - axial velocity